



Durham E-Theses

A theoretical study towards proton transfer in N-methylacetamide

Amer, Halima

How to cite:

Amer, Halima (1997) *A theoretical study towards proton transfer in N-methylacetamide*, Durham theses, Durham University. Available at Durham E-Theses Online: <http://etheses.dur.ac.uk/5463/>

Use policy

The full-text may be used and/or reproduced, and given to third parties in any format or medium, without prior permission or charge, for personal research or study, educational, or not-for-profit purposes provided that:

- a full bibliographic reference is made to the original source
- a [link](#) is made to the metadata record in Durham E-Theses
- the full-text is not changed in any way

The full-text must not be sold in any format or medium without the formal permission of the copyright holders.

Please consult the [full Durham E-Theses policy](#) for further details.

**A Theoretical Study Towards
Proton Transfer in
N-methylacetamide**

Halima Amer

Thesis submitted for the degree of
Master of Science

University of Durham
Department of Chemistry

September 1997

The copyright of this thesis rests
with the author. No quotation
from it should be published
without the written consent of the
author and information derived
from it should be acknowledged.



1 DEC 1998

ABSTRACT

Vibrational spectroscopy with Inelastic Neutron Scattering has indicated that proton transfer occurs along the hydrogen bond in *N*-methylacetamide and that this transfer is governed by a double minimum potential.¹ Models of the system have been investigated further by *ab initio* calculations, and the electrostatic potentials around the models determined. As a result, the nature of the potential well has been characterised and the dynamics of the proton transfer have been investigated more fully. The effect of increasing the separation between the hydrogen bonded units on the potential well has been studied, as well as the effect of increasing the number of units. These analyses have provided useful insights into what is already known about the proton transfer dynamics of the system and have facilitated a comparison with the experimental spectroscopic data.

- [1] Kearley, G. J., Fillaux, F., Baron, M.-H., Bennington, S., Tomkinson, J. *Science* **264**, 1285, (1994)

DECLARATION

The work described in this thesis was carried out at the University of Durham between October 1996 and September 1997. This work has not been submitted, either completely or in part, for a degree in this or any other University and is the original work of the author except where acknowledged by reference.

The copyright of this thesis rests with the author. No quotation from it should be published without their prior written consent and information derived from it should be acknowledged.

For my mother and father

“I wish to God these calculations had been executed by steam”

Charles Babbage, 1792-1871

ACKNOWLEDGEMENTS

- Professor Judith Howard** For advice, support and endless patience
- Dr. Frank Allen** For supplying funding, energy and helpful suggestions
- Dr. Sally Price** For invaluable help and considerable amounts of time
- Professor Jeremy Hutson** For many illuminating discussions and again, considerable amounts of time
- Dr. Garry Smith** For good ideas, and for troubleshooting
- Dr. Jos Lommerse** For help with CADPAC
- Clair, Gus and Carl** For too many things to mention
- Ginn, Andy, Jenny,** For everything else
- Jody and Amanda**

Thanks also go to the EPSRC for funding this project.

CONTENTS

CHAPTER 1: Introduction	1
1.1 Proton Transfer	1
1.2 Previous Studies of Proton Transfer in <i>N</i>-methylacetamide	4
1.3 A Theoretical Approach	7
1.4 References	9
CHAPTER 2: <i>Ab Initio</i> Calculations	11
2.1 Theory	11
2.1.1 Schrödinger's equation	11
2.1.2 Self-consistent field theory	15
2.1.3 Electron correlation	24
2.2 Methodology	28
2.2.1 Procedure.	28
2.2.2 Computation	29
2.3 Results and Discussion	31
2.3.1 Formamide	31
2.3.2 The (methyl)acetamide dimer	33
2.3.3 The (methyl)acetamide trimer	58
2.3.4 The (methyl)acetamide tetramer	60
2.3.5 The (methyl)acetamide pentamer	62
2.4 References	65

CHAPTER 3: Distributed Multipole Electrostatic Models	67
3.1 Theory	67
3.1.1 The electrostatic potential	67
3.1.2 Distributed multipole models of the electrostatic potential	68
3.2 Methodology	71
3.2.1 Procedure	71
3.2.2 Computation	73
3.3 Results and Discussion	74
3.3.1 Additivity of the monomer units	74
3.3.2 Is there cooperativity between two or more protons?	80
3.3.3 Stability of the system to the movement of the proton.	93
3.4 References	96
CHAPTER 4: Conclusions	97
CHAPTER 5: Additional Work: A theoretical study of the hydrogen bond acceptor properties of divalent sulfur and oxygen	100
5.1 Introduction	100
5.1.1 Previous work	100

5.1.2	IMPT calculations of the acceptor properties of C=S and C=O systems	107
5.2	Methodology	108
5.2.1	Procedure	108
5.2.2	Computation	111
5.3	Results and Discussion	112
5.4	Conclusions	120
5.5	References	121
APPENDIX:	Conferences and Courses	122
I	Conferences	122
II	Courses	123
III	Time Spent Away from Durham	124

CHAPTER 1

Introduction

1.1 Proton Transfer

Proton transfer reactions have been described as “one of the most important classes of chemical reactions in solution”.¹ They are central to processes such as acid-base neutralisations, enzymatic reactions and physical processes such as collective hydrogen atom transfer in solid-state hydrogen bonded networks. Proton transfer reactions are consequently of great interest to chemists, biologists and physicists.² Considerable research has gone into understanding the reaction mechanisms and the subsequent implications of any findings, drawing on a wide range of experimental and theoretical techniques to achieve this.³⁻¹²

The typical path of a proton transfer reaction in a one-dimensional hydrogen bonded chain is as follows:



where X and Y denote ions or aggregates and H is a hydrogen atom that is bonded covalently or ionically with an adjacent ion (solid line) and forms a hydrogen bond with another ion (dotted line).⁶ Accompanying the transfer of the proton is a shift of electron density in the opposite direction.¹³ The reaction may be intramolecular or intermolecular, can be activated thermally or by photoinduction and may be a barrierless process or occur by quantum tunnelling.¹⁴ A crucial feature in proton transfer is electron coupling between the proton donor and acceptor. For poorly hydrogen bonded systems and rigid intramolecular proton transfer systems, this coupling is weak and the proton dynamics are dominated by tunnelling. Systems where the proton is involved in strong hydrogen bonds between N or O donor and acceptor groups impose classical behaviour on the dynamics of the transfer and the proton must pass over the barrier for transfer to take place.³

Marcus theory not only relates geometrical and thermodynamic parameters to reaction mechanisms but also provides an established model in which proton transfer can be predicted based on parameter values.¹⁸ Hence if the potential energy profile of an intermolecularly bonded system is known, then whether or not proton transfer is likely to take place along a hydrogen bond can be evaluated. As well as this, the most favourable conditions to allow this transfer can be assessed, and so a dynamic picture of the mechanism of proton transfer can be built up from energetic information about the static system.

1.2 Previous Studies of Proton Transfer in *N*-methylacetamide

N-methylacetamide, $\text{CH}_3\text{CONHCH}_3$, is an ideal candidate for an investigation of proton transfer in amides. It is a simple model for the peptide unit, and so studies on *N*-methylacetamide act as a foundation for analyses of proton transfer in polypeptides and proteins. The crystal structure of *N*-methylacetamide was determined in 1960,¹⁹ and was found to exist in two forms. Below 283 K, it exists as

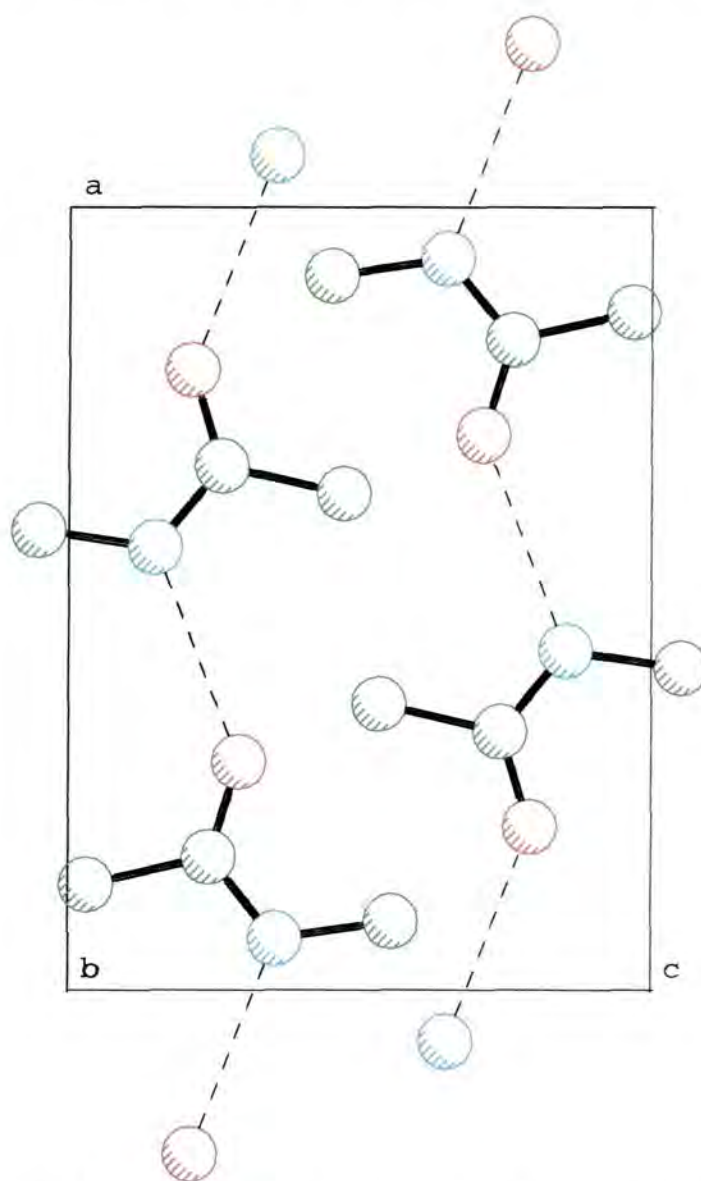


Figure 1.2 Crystal packing diagram of the low-temperature form of *N*-methylacetamide (key: C atoms – green, O atoms – red, N atoms – blue). The hydrogen bonded distance is 2.825 Å, and the angle C–N...O is 140.8°.¹⁹

molecular chains with four molecules per unit cell, with dimensions $a = 9.61$, $b = 6.52$, $c = 7.52$ Å. The space group is *Pnma* (figure 1.2). At 283 K, n-methylacetamide undergoes a phase transition and the resulting high-temperature form has only two molecules per unit cell, which has dimensions $a = 4.85$, $b = 6.59$, $c = 7.30$ Å. The space group for the high-temperature form is *Pnmm*. Hydrogen bonding is preserved above the phase transition.

Vibrational spectroscopy has been used extensively to examine proton transfer dynamics in *N*-methylacetamide.²⁰ The infrared spectra of both *N*-methylacetamide and the deuterated compound have been obtained for the low-temperature crystals, pure liquids and solutions in various solvents.²¹ The spectra for all three phases of *N*-methylacetamide suggest that the fundamental mode of the non-deuterated compound is described by a double minimum potential, evidence for proton transfer occurring in *N*-methylacetamide. Other studies have provided further valuable information about the dynamics of the proton transfer, showing that the N—H bond undergoes significant weakening during the process, revealing that the hydrogen bond is ionic in character ($N^{\delta-} \dots H^+ \dots O^{\delta-}$) as is the case in hydrogen bonded ionic crystals.²²

Vibrational spectroscopy has also shown that there is a dynamical exchange between two configurations of *N*-methylacetamide, an amide-like form (...OCNH...) and an imidol-like form (...HOCN...). At room temperature, both configurations are equally likely and the proton transfer is governed by a symmetric double minimum potential. At low temperatures (below 20 K), the imidol form is more likely and the potential is asymmetric. Proton transfer, therefore, can be seen to occur as a natural consequence of hydrogen bond formation in this case.²² However, the results of these vibrational analyses have been the source of controversy due to the “nonspecific

sensitivity for the proton vibrations and the lack of a rigorous theoretical framework for the interpretation of observed intensities”.¹

Subsequent studies have incorporated inelastic neutron scattering (INS) with vibrational spectra,^{22,23} and this approach has facilitated a dynamical analysis of the mechanism of proton transfer in *N*-methylacetamide. As neutrons are used to excite vibrations instead of photons as in optical spectroscopy, the same transitions are observed but with different intensities as they are attributable solely to nuclear motions. These intensities are related to the atomic displacements which are scaled to the nuclear cross sections, and as protons have large cross sections (almost 10 times greater than for any other atom), the proton dynamics can be studied in detail and on a time scale comparable to the dynamics of the proton transfer.

As with earlier studies, the results of the spectroscopic analysis with INS, although consistent with recent work involving Neutron Compton scattering measurements,^{24,25} are not “...conclusive for the proton dynamics [in *N*-methylacetamide]”,¹ and in any case vibrational spectroscopy cannot be used to determine the exact location of the double minimum. The exact nature of the proton transfer dynamics in *N*-methylacetamide have yet to be determined by spectroscopic studies, and a combination of theoretical and experimental data from a variety of techniques is necessary to provide a full picture of the process involved.

1.3 A Theoretical Approach

It is evident that more data from experimental and theoretical techniques is needed to investigate thoroughly the nature of the proton transfer in *N*-methylacetamide. The approach taken in this work has concentrated on using *ab initio* calculations to obtain the energies of the system for different positions of the hydrogen atom along the N...O vector for fixed monomer geometries placed relative to each other as in the crystal structure¹⁹ in the dimer and in the trimer, tetramer and pentamer molecules in an attempt to simulate the crystalline environment.

Theoretical studies of proton transfer dynamics have tended to favour a classical approach, using Marcus theory to determine the reaction parameters.^{2,3,6,7,13,14} More recent analyses, though, have attempted to apply quantum-dynamical methods to investigate proton transfer processes^{5,7,9,10,11,26} with varying degrees of success in explaining the mechanism of the dynamics. The most promising technique has been the use of *ab initio* calculations, as it is possible to calculate not only the absolute energies but to examine the variation of atomic charges thus obtained during the proton transfer.⁵

Although it is not possible to obtain a 'real-time' picture of the transfer with *ab initio* calculations, which is the case with vibrational spectroscopy and some quantum-classical simulations invoking the time-dependent Schrödinger equation, it is possible to simulate the dynamics of proton transfer by performing *ab initio* calculations for different molecular geometries and thus build up a step-by-step energy profile for different hydrogen atom positions along the vector.

Similarly, it is possible to calculate the electrostatic potential around molecules and investigate the effect on the potential of moving a hydrogen atom along a donor-

acceptor vector.^{27,28} This technique, also based on the *ab initio* calculation of molecular wavefunctions, can be used to describe the movement of electron density as the proton is moved, thus simulating the effects of a crystal field and allowing an assessment of the additivity of the monomer units and the cooperativity of the motion of the protons where more than one hydrogen bond is present.²⁶

The results from such theoretical studies allow a comprehensive study of the proton dynamics in hydrogen bonded system to be made. Such a combined theoretical analysis will not only give a clearer view of the proton dynamics in this simple system but will also allow a comparison of the data from these theoretical techniques with that from the experimental spectroscopic methods to be made. In this way, the role of such theoretical techniques in understanding a dynamical process such as proton transfer can be assessed.

1.4 References

- [1] Formosinho, S. J. *J. Chem. Soc. Perkin Trans. II* **61**, (1987)
- [2] Kuznetsov, M., Ulstrup, J. *J. Chem. Phys.* **188**, 131, (1984)
- [3] Kearley, G. J., Fillaux, F., Baron, M.-H., Bennington, S., Tomkinson, J. *Science* **264**, 1285, (1994)
- [4] Olovsson, I. *Z. Kristallogr.* **182**, (1-4), 203, (1994)
- [5] Florian, J., Scheiner, S. *J. Comp. Chem.* **15**, (5), 533, (1994)
- [6] Mei, Y. P., Yan, J. R., Yan, X. H., You, J. Q. *Phys. Rev. B* **48**, (1), 577, (1993)
- [7] Bala, P., Grochowski, P., Lesyng, B., McCammon, J. A. *J. Phys. Chem.* **100**, 2535, (1996)
- [8] Isaacson, A. D., Scheiner, S., Wang, L. *J. Phys. Chem.* **97**, 1765, (1993)
- [9] Grauer, R., Spatschek, K. H., Zolotaryuk, A. V. *Phys. Rev. E* **47**, (1), 236, (1993)
- [10] Chu, C.-H., Ho, J.-J. *J. Phys. Chem.* **99**, 1151, (1995)
- [11] Barclay, V. J., Dateo, C. E., Hamilton, I. P. *J. Chem. Phys.* **101**, (8), 6766, (1994)
- [12] Pérez, P., Contreras, R. *Chem. Phys. Lett.* **256**, (15), (1996)
- [13] Keifer, P. M., Leite, V. B. P., Whitwell, R. M. *Chem. Phys.* **194**, 33, (1995)
- [14] Douhal, A., Lahmani, F., Zewail, A. H. *Chem. Phys.* **207**, 477, (1996)
- [15] Graf, F., Meyer, R., Ha, T.-K., Ernst, R. R. *J. Chem. Phys.* **75**, (6), 2914, (1981)
- [16] Meier, B. H., Graf, F., Ernst, R. R. *J. Chem. Phys.* **76**, (2), 767, (1982)
- [17] Meyer, R., Ernst, R. R. *J. Chem. Phys.* **86**, (2), 784, (1987)

- [18] Marcus, R. A. *Ann. Rev. Phys. Chem.* **15**, 155, (1964)
- [19] Katz, J. L., Post, B. *Acta Cryst.* **13**, 624, (1960)
- [20] Tomkinson, J., Kearley, G. J., Fillaux, F. *Physica B* **174**, 246, (1991)
- [21] Fillaux, F., Baron, M.-H. *Chem. Phys.* **62**, 275, (1981)
- [22] Fillaux, F., Fontaine, J. P., Baron, M.-H., Kearley, G. J., Tomkinson, J. *Chem. Phys.* **176**, 249, (1993)
- [23] Fillaux, F., Fontaine, J. P., Baron, M.-H., Kearley, G. J., Tomkinson, J. *Physica B* **180**, 683, (1993)
- [24] F. Fillaux *ISIS Experimental Report A* **278**, (June 1994)
- [25] Fillaux, F., Baron, M.-H., Mayers, J., Tomkinson, J. *Chem. Phys. Lett.* **240**, 114, (1995)
- [26] Scheiner, S., Yi, M. *J. Phys. Chem.* **100**, 9235, (1996)
- [27] Stone, A. J. *Chem. Phys. Lett.* **83**, 233, (1981)
- [28] S. L. Price, 'Electrostatic forces in molecular interactions' in "*Molecular Interactions: From van der Waals to Strongly Bound Complexes*" ed. S. Scheiner, (Wiley, 1997)

CHAPTER 2

***Ab Initio* Calculations**

2.1 Theory

2.1.1 Schrödinger's equation

"The underlying physical laws necessary for the mathematical theory of a large part of physics and the whole of chemistry are...completely known, and the difficulty is only that the exact application of these laws leads to equations much too complicated to be soluble."

Paul Dirac, 1929

The Schrödinger equation is the basis of all *ab initio* calculations. Using the time-independent form of the equation (*equation 2.1*), it is possible in principle to determine exactly the structural, energetic and geometric properties of any molecule.¹

$$H\Psi = E\Psi \quad (2.1)$$

where E is the total molecular energy,

Ψ is the total molecular wavefunction,

H is the molecular Hamiltonian operator.

In practice, however, it is not possible to obtain an exact solution of Schrödinger's equation and so a number of simplifying approximations must be made.

The Born-Oppenheimer approximation

The Born-Oppenheimer approximation simplifies the solution of Schrödinger's equation by assuming that the motion of atomic nuclei is negligible when compared to the movement of electrons. This assumption is valid because of the large mass ratio between electrons and nuclei. Using this approximation, the Schrödinger equation can be solved using the electronic wavefunction and electronic

Hamiltonian operator to calculate the potential energy function of a system in the field of the stationary atomic nuclei, and so the potential energy surface can be obtained.

The Hamiltonian operator

The Hamiltonian operator for an electron i is defined by *equation 2.2*,

$$H = -\frac{\hbar^2}{2m} \nabla^2(i) + V(i) \quad (2.2)$$

In a simpler form, this can be expressed as

$$H = T + V \quad (2.3)$$

where T is the kinetic energy operator,

V is the potential energy in the field of the nuclei and all the electrons.

The kinetic energy is the summation of the differential operator ∇^2 over the entire molecule (*equation 2.4*),

$$T = -\frac{\hbar^2}{8\pi^2} \sum_{i=1}^N \frac{1}{m_i} \left(\frac{\partial^2}{\partial x_i^2} + \frac{\partial^2}{\partial y_i^2} + \frac{\partial^2}{\partial z_i^2} \right) \quad (2.4)$$

The potential energy component is the Coulombic repulsion between pairs of charged particles (*equation 2.5*),

$$V = \frac{1}{4\pi\epsilon_0} \sum_i \sum_{j<i} \frac{e_i e_j}{r_{ij}} \quad (2.5)$$

where r_{ij} is the distance between the two particles,

e_i, e_j are the charges on particles i and j .

This term can further be reduced to a summation of attractive and repulsive terms (*equation 2.6*),

$$V = \frac{1}{4\pi\epsilon_0} \left(- \sum_i^{\text{electrons}} \sum_I^{\text{nuclei}} \left(\frac{Z_I e^2}{r_{iI}} \right) + \sum_i^{\text{electrons}} \sum_{j<i} \left(\frac{e^2}{r_{ij}} \right) + \sum_I^{\text{nuclei}} \sum_{J<I} \left(\frac{Z_I Z_J e^2}{R_{IJ}} \right) \right) \quad (2.6)$$

The first term in the equation describes attraction between electrons and nuclei, the second term repulsion between electrons and the third term repulsion between nuclei. The Born-Oppenheimer approximation means that the kinetic energy of the nuclei can be neglected, and so the electronic Hamiltonian can be written in atomic units (energies in Hartrees) as follows (equations 2.7, 2.8),²

$$H^{elec} = T^{elec}(\vec{r}) + V^{nucl-elec}(\vec{R}, \vec{r}) + V^{elec}(\vec{r}) + V^{nucl}(\vec{R}) \quad (2.7)$$

$$H^{elec} = -\frac{1}{2} \sum_i^{\text{electrons}} \left(\frac{\partial^2}{\partial x_i^2} + \frac{\partial^2}{\partial y_i^2} + \frac{\partial^2}{\partial z_i^2} \right) - \sum_i^{\text{electrons}} \sum_I^{\text{nuclei}} \left(\frac{Z_I}{|\vec{R}_I - \vec{r}_i|} \right) + \sum_i^{\text{electrons}} \sum_{j<i} \left(\frac{1}{|\vec{r}_i - \vec{r}_j|} \right) + \sum_I^{\text{nuclei}} \sum_{J<I} \left(\frac{Z_I Z_J}{|\vec{R}_I - \vec{R}_J|} \right) \quad (2.8)$$

The electronic wavefunction

There are a number of restrictions that apply to the electronic wavefunction to enable its use in the solution of the Schrödinger equation for the potential energy. These are the following:

- i. The wavefunction must be normalised, that is the probability that electron(s) exist must be equal to one (equation 2.9).

$$\int |\Psi|^2 d\tau = 1 \quad (2.9)$$

- ii. The eigenfunction solutions to equation 2.1 corresponding to different energy values E_i, E_k must be orthogonal (equation 2.10).

$$\int \Psi_i \Psi_k d\tau = 0 \quad (2.10)$$

- iii. The wavefunction must be finite at all points in space.

- iv. The wavefunction must be single-valued at all points in space.
- v. The wavefunction must be continuous at all points in space.

As long as these restrictions are satisfied, the electronic wavefunction can be used in the Schrödinger equation with the electronic Hamiltonian to obtain the effective potential energy for a system.¹

2.1.2 Self-consistent field theory

Even with approximations made to the Schrödinger equation, it is not possible to solve it for anything but the simplest molecular systems.² Self-consistent field (SCF) theory, based on formalisms developed by Hartree and Fock, contains a number of assumptions that enable molecular properties to be obtained for ‘real-life’ molecular systems.

Molecular orbitals

For many-electron wavefunctions, the solution to the Schrödinger equation is based in expressing the wavefunction as a combination of spin orbitals. These are the product of molecular orbitals and spin functions and the wavefunction is found by expanding the spin orbitals in a Slater determinant (*equation 2.11*). This is the fundamental unit for a molecular electronic structure calculation.

$$\Psi = \frac{1}{\sqrt{N!}} \begin{vmatrix} \psi_1(1)\alpha(1) & \psi_1(1)\beta(1) & \dots & \psi_1(n)\alpha(n) & \psi_1(n)\beta(n) \\ \psi_2(1)\alpha(1) & \psi_2(1)\beta(1) & \dots & \psi_2(n)\alpha(n) & \psi_2(n)\beta(n) \\ \vdots & \vdots & & & \\ \psi_n(1)\alpha(1) & \psi_n(1)\beta(1) & \dots & \psi_n(n)\alpha(n) & \psi_n(n)\beta(n) \end{vmatrix} \quad (2.11)$$

where $\psi_1\psi_2\dots\psi_n$ are the molecular orbitals,

α, β are spin functions for up and down electrons respectively,

n is the number of electrons.

The determinant obeys the Pauli principle in that the wavefunctions change sign when the coordinates of two electrons interchange³ – the wavefunctions obey the anti-symmetry principle. The molecular orbitals are approximated by a Linear Combination of Atomic Orbitals (LCAO) method. The atomic orbitals are one electron ‘basis functions’ from which the molecular orbitals are derived (*equation 2.12*),

$$\psi_i = \sum_{k=1}^n C_{ik} \phi_k \quad (2.12)$$

where C_{ik} are the molecular orbital expansion coefficients.

This is the closed-shell method. For systems with unusual electronic structures, unpaired electrons or systems in which there is bond dissociation it is necessary to treat the systems as having open shells. Open-shell methods allow unpaired electrons to occupy orbitals separately by considering two sets of molecular expansion coefficients instead of one. For electrons alpha and beta to be considered in separate orbitals, this means that the following relationships will apply:

$$\psi_i^\alpha = \sum_{k=1}^n C_{ik}^\alpha \phi_k \quad (2.13)$$

$$\psi_i^\beta = \sum_{k=1}^n C_{ik}^\beta \phi_k \quad (2.14)$$

Two sets of orbital coefficients are obtained, which ultimately result in two sets of molecular orbitals which can then describe the electrons separately.²

The variational principle

To obtain a solution for the molecular orbitals and hence the molecular wavefunction it is necessary to solve for the molecular orbital expansion coefficients. To do this, the variational principle is used, and this states that any approximate wavefunction will always be of a higher energy than the exact wavefunction, and therefore the wavefunction giving the lowest energy is the best approximation to the exact solution.⁴ This is expressed in *equations 2.15* and *2.16*,

$$E_{approx} = \int \frac{\psi^* H \psi d\tau}{\psi^* \psi d\tau} \quad (2.15)$$

$$\frac{\partial E_{approx}}{\partial C_{ik}} = 0 \quad (2.16)$$

To satisfy the variational principle, the condition in *equation 2.16* must apply.

The Hartree-Fock equations

The condition of the variational principle leads to the derivation of the Hartree-Fock equations (*equation 2.17*),

$$\hat{F}(1)\phi_i(1) = \varepsilon_i\phi_i(1) \quad (2.17)$$

where the Fock operator is defined by (*equation 2.18*)

$$\hat{F}(1) = \hat{H}_{(1)}^{\text{core}} + \sum_{j=1}^{n/2} [2\hat{J}_j(1) - \hat{K}_j(1)] \quad (2.18)$$

and

$$\hat{H}_{(1)}^{\text{core}} \equiv -\frac{1}{2}\nabla_1^2 - \sum_{\alpha} \frac{Z_{\alpha}}{r_{1\alpha}} \quad (2.19)$$

where the Coulomb operator \hat{J}_j and the exchange operator \hat{K}_j are defined by

$$\hat{J}_i(1)f(1) = f(1) \int |\phi_j(2)|^2 \frac{1}{r_{12}} dv_2 \quad (2.20)$$

$$\hat{K}_i(1)f(1) = \phi_j(1) \int \frac{\phi_j^*(2)f(2)}{r_{12}} dv_2 \quad (2.21)$$

The Fock operator (*equation 2.18*) is calculated by an evaluation of one- and two-electron integrals, which give contributions to the kinetic energy of the electron-nuclear attraction and electron-electron repulsions respectively. This procedure is carried out iteratively until the difference in energy is so small that it can be assumed that convergence has occurred and the field is self-consistent.⁴

Basis sets

The basis functions used in *equation 2.12* to evaluate the molecular orbitals by the LCAO method comprise a basis set. If there were an infinite number of basis functions, the wavefunction would be solved at the Hartree-Fock limit. Limitations

on computing time mean that it is not possible to use an infinite basis set, and so approximations must be applied. There are standard basis sets available with any program used for *ab initio* calculations, and the choice of basis set will depend on the accuracy required.

Basis sets can be broadly categorised according to whether they use Slater-type orbitals (STO's) or Gaussian-type orbitals (GTO's). STO's are of the general form

$$\phi_i = F_n(r)Y_{lm}(\theta, \phi)w(s) \quad (2.22)$$

where

$$F_n(r) = C_n r^{n-1} e^{-\zeta r} \quad (2.23)$$

where $F_n(r)$ is the radial function,

n corresponds to the principal quantum number,

ζ is an exponent that depends on the angular momentum quantum number l ,

the spherical harmonics $Y_{lm}(\theta, \phi)$ are eigenfunctions of the operator for the

square of the orbital angular momentum of an electron, \hat{L}^2 ,

w is a spin function α or β .⁵

STO's are correct for atomic orbitals and describe electron density near the nucleus well. They are flexible functions, and so are good for the construction of wavefunctions. However, their use leads to difficulties in the calculation of one- and two-electron integrals, resulting in computational difficulties.

GTO's are described by the following function (equation 2.24),

$$\phi_i = Nx^L y^M z^N e^{-\alpha r^2} \quad (2.24)$$

When $L + M + N = 0$ the GTO is an s-type Gaussian, $L + M + N = 1$ a p-type Gaussian and $L + M + N = 2$ a d-type Gaussian *etc.*⁵ GTO's are preferable to STO's for molecular calculations because the integrals involving them can be solved

analytically, and the methods for doing this are very efficient. A problem with GTO's, however, is that they fall off rapidly with the distance from the nucleus and so do not mimic electronic behaviour as well as STO's. If enough GTO's are used in a linear combination, they mimic STO's accurately enough for the computational benefits of their use to favour them over STO's.²

Standard basis sets can be classified as follows:

Minimal basis sets

In a minimal basis set such as STO-3G only the minimum number of basis functions for each atom are present. The atoms are described by STO's containing three Gaussian primitives per basis function ('3G').

Split valence basis sets

Double split valence sets such as 3-21G are larger than the minimal basis sets. The core orbitals are described by three Gaussian primitives, as in the minimal STO-3G basis set, but the valence orbitals are described by two functions and an additional diffuse primitive Gaussian.

Triple split valence sets such as 6-311G contain six primitive functions describing the core orbitals and three functions for each valence orbital. There are also two additional diffuse primitive Gaussians describing the valence orbitals.

Extended basis sets

Extended basis sets are split valence basis sets that have additional polarisation functions or diffuse functions on the orbitals.

Polarised basis sets remove the limitation imposed on the shape of the valence orbitals (*equation 2.20*) by adding orbitals with angular momenta greater than those needed to describe the molecular ground state orbital shape. Examples of these would be *d*-functions on carbon atoms and *p*-functions on hydrogen atoms. These basis sets have been shown to give more accurate results for calculations of electronic properties, and are used widely in high-level calculations.⁶⁻¹⁰

Diffuse functions are similar to polarisation functions in that they allow the valence orbitals to occupy a greater region of space. They are large *s*- and *p*-type functions and have a considerable effect in reducing basis set superposition error (below).¹¹ They are used for high-level calculations where valence-electronic effects are of particular interest.²

Polarisation and diffuse functions could be added only to atoms involved in a particular bond or on heavy atoms to reduce computing time. In this way it is possible to customise basis sets depending on the specific property required from the calculation. This allows computing time to be concentrated on areas of particular interest, and can lead to more accurate calculations as a consequence.

Basis set superposition error (BSSE)

A problem with calculating properties of molecular donor-acceptor complexes or supermolecules is that standard basis sets are too contracted around the nucleus and so a description of the electronic lone pair orbitals around the acceptor atoms in a hydrogen bonded complex is inadequate. As a consequence, there is increased stabilisation of one monomer due to the presence of basis functions on the other – the basis set superposition error (BSSE).¹² For calculations on such a system,

the equilibrium monomer distance will often be too short and the minima too deep unless this effect is corrected for. There are several ways to do this:

Counterpoise corrections

The problem of BSSE in supermolecule calculations can be addressed by using the Boys-Bernardi counterpoise method.¹³ The scheme takes account of the unoccupied or ‘ghost’ orbitals on the first monomer that are accessible to the electrons of the second, and corrects for BSSE by allowing these orbitals to be occupied by the lone pairs of the second monomer. This method is described as a ‘full’ counterpoise correction.

The procedure involves subtracting from the energy of the entire complex the energies of the separate molecules obtained by using the basis sets of both molecules, which gives the corrected supermolecule energy. The counterpoise correction is obtained by subtracting from this the uncorrected supermolecule energy, which is simply the difference between the complex energy and the energies of the individual molecules using only their basis sets.

This can be represented for two bound molecular units A and B by the following relationships (*equations 2.25 and 2.26*),

$$E_{AB}^0 = V_{AB}(AB) - V_A(A) - V_B(B) \quad (2.25)$$

$$E_{AB}^{CP} = V_{AB}(AB) - V_A(AB) - V_B(AB) \quad (2.26)$$

where E_{AB}^0 is the uncorrected supermolecule energy,

E_{AB}^{CP} is the counterpoise-corrected supermolecule energy,

$V_{AB}(AB)$ is the energy of the entire complex,

$V_A(AB)$, $V_B(AB)$ are the energies of the molecules A and B respectively, using the basis sets of both to obtain the corrected energies,

$V_A(A)$, $V_B(B)$ are the energies of the molecules A and B respectively, using only their respective basis sets in the calculations.

The counterpoise-corrected energy can be represented as follows (*equation 2.27*),

$$E_{AB}^{CP} - E_{AB}^0 = [V_A(A) + V_B(B)] - [V_A(AB) + V_B(AB)] \quad (2.27)$$

The counterpoise-corrected energy is usually of a few kJ mol^{-1} for larger basis sets, with larger values obtained for poorer basis sets. However, for very poor basis sets, the value of the counterpoise correction has been questioned, with only more complete basis sets yielding reliable results. As basis sets become more complete, so too should the correction diminish – provided the basis sets are adequate in the first instance.¹⁴

The application of the full counterpoise correction scheme has been a matter of some controversy, and this has led to the development of the virtuals-only counterpoise scheme. This differs from the full counterpoise correction in that only the virtual orbitals of one monomer are made available to the other and not the ghost orbitals.¹² This means that stabilisation due to the mixing of one monomer's orbitals with the others is not possible.

The merits of the full counterpoise recipe relative to the virtuals-only one has been the subject of much debate, but it has been shown that the full counterpoise scheme results in an improvement in the agreement between the corrected result and the Hartree-Fock limit, which would be expected.¹⁵ The virtuals-only counterpoise correction does not show this improvement, which suggests that the best scheme to correct for BSSE is the Boys-Bernardi one. However, in many cases it is more useful to consider the correction as a marker for the reliability of the result rather than an absolute value.

Addition of polarisation functions to basis sets

If the basis sets used in the calculation are large enough with sufficient polarisation functions to adequately describe the atomic orbitals, the monomer energies will be close enough to the basis set limit so that the effect of the second monomer's basis functions is negligibly small.¹² It has also been suggested that putting diffuse functions on the orbitals will further minimise BSSE.¹⁶

2.1.3 Electron correlation

SCF theory does not allow for correlation between electrons. The wavefunction depends only on absolute electron coordinates and not on the distance between them, resulting in the electrons being considered independently of each other. The energy associated with this effect, ‘correlation energy’ is not insignificant, and so energies calculated by SCF methods are higher than they should be, typically by 0.5-1.0% of the SCF energy.⁵ There are a number of theoretical techniques that attempt to account for electron correlation effects in *ab initio* calculations.

Möller-Plesset perturbation theory

This is a simple way of accounting for electron correlation effects and is widely used in *ab initio* calculations. The basis of the theory rests on dividing the Hamiltonian operator for a system into two parts, a known Hamiltonian operator and a perturbing Hamiltonian (*equation 2.28*),

$$H = H_0 + \lambda H_1 \quad (2.28)$$

where H_0 is the known operator,

H_1 is the perturbing Hamiltonian.

This perturbing Hamiltonian is used to calculate the perturbed wavefunction and energy, and these are substituted into the Schrödinger equation. The resulting products can be expanded to give coefficients that can be equated for powers of λ , giving a series of relations for each order of perturbation. In this way, energy corrections of the second, third and fourth order can be calculated.²

Configuration interaction theory

Instead of modifying the Hamiltonian, Configuration interaction (CI) theory is based on the premise that as the wavefunction cannot be expressed exactly by a single determinant, it is necessary to substitute one or more occupied orbitals in the Slater determinant with a virtual orbital to take account of the effect of electron correlation.

In the full CI method, the wavefunction is expressed as follows (equation 2.29):

$$\Psi = b_0\Psi_0 + \sum_{s>0} b_s\Psi_s \quad (2.29)$$

where b_0, b_s are coefficients to be solved for by minimising the energy of the resultant wavefunction.

The first term is at the Hartree-Fock level, and the second term sums over all possible substituted determinants. For larger basis sets, this method allows the Schrödinger equation to be solved more accurately, and as the basis set becomes infinite, the solution becomes exact.²

As this method is very slowly convergent, very large basis sets are needed to generate a sufficiently large number of virtual orbitals.³ Limited CI is therefore used for larger systems, and in this case only a limited number of orbitals are substituted in the Slater determinant.

Density functional theory

Density functional theory (DFT) is based on the theorem that the electron density of a system is all that is needed to compute the energy. This is the Hohenberg-Kohn theorem, and it states that “*the energy is a functional of the*

density".¹⁷ To calculate electron correlation, the electronic energy is divided into the following terms (equation 2.30):

$$E = E^T + E^V + E^J + E^{XC} \quad (2.30)$$

where E^T is the kinetic energy term,

E^V is the potential energy term,

E^J is the electron-electron repulsion term,

E^{XC} is the exchange correlation term.

All these terms are functionals of the electron density. The exchange correlation term can be further divided into exchange functionals and correlation functionals, and DFT methods are based on pairing these functionals together.³ Traditional functionals are divided into two groups:

Local functionals

These only involve the values of the electron spin densities. Examples of local exchange functionals include the Slater and X_∞ functionals, and the Vosko-Wilk-Nusair (VWN) is a commonly used local correlation functional.²

Gradient-corrected (non-local) functionals

These involve the values of the electron spin densities and their gradients. A widely used method is the BLYP combination of the Becke exchange functional and the Lee, Yang and Parr correlation functional.²

There are also hybrid functionals consisting of a linear combination of HF, local and gradient-corrected exchange functionals. These are then used in

conjunction with either local or gradient-corrected correlation functionals. An example of this is the B3LYP formulation.²

An advantage of DFT is that it is less computing-intensive than other correlation methods. However, the method has been shown to be inadequate as far as calculations on hydrogen-bonded complexes are concerned.¹⁸

2.2 Methodology

2.2.1 Procedure

Ab initio calculations were performed on the (methyl)acetamide monomer, dimer, trimer, tetramer and pentamer, and a further series of calculations were done on the dimer for different monomer separations. As a first step, the monomer geometries were optimised and these units placed together in the larger molecules at the crystallographically defined N...O separation and C–N...O angle, 2.825 Å and 140.8° respectively (*figure 1.2*).¹⁹ The subsequent energy calculations on the dimer, trimer, tetramer and pentamer were performed on these fixed molecular geometries. To reduce the amount of computing time needed for the calculations, the methyl groups were substituted by hydrogen atoms, and this approximation is taken into account when analysing the results.

The energies of the fixed geometries were obtained in each case for different hydrogen atom positions along the N...O vector, keeping the heavy atom positions fixed. The hydrogen atoms were moved in 0.05 Å increments to give sufficiently high resolution to the resulting potential energy curves. For the trimer, tetramer and pentamer the hydrogen atoms were moved simultaneously and in the same direction. The effect of increasing the monomer separation was also investigated, with series of calculations performed on the dimer for monomer separations 0.2 Å, 0.4 Å, 0.6 Å, 0.8 Å and 1.0 Å greater than those observed crystallographically.

The calculated energies for the dimer were corrected for BSSE using the Boys-Bernardi counterpoise method.^{13,14}

2.2.2 Computation

The programs *GAMESS (General Atomic and Molecular Electronic Structure System, VMS version, November 1995)*²⁰ and *CADPAC (Cambridge Analytical Derivatives Package, UNIX version, issue 6)*²¹ were both used for the computation. The programs were run on DEC-Alpha and Silicon Graphics IRIX version 6.2 platforms respectively. Both *GAMESS* and *CADPAC* are extensively used for small molecule calculations. These *ab initio* programs use an iterative process to compute solutions to the Schrödinger equation using the mathematical approximations outlined in *section 2.1*. In this case, the programs were used to optimise molecular geometries and obtain molecular energies at different levels of theory.

The unconstrained monomer geometry was optimised using both *GAMESS* and *CADPAC*, and a series of calculations done on this unit using basis sets 3-21G* and 6-31G* at the SCF level and 6-311G** at the MP2 level. The final optimised monomer geometry from the results of the calculation using the 6-311G** basis set at the MP2 level used in subsequent calculations was obtained with *GAMESS*. Calculations on the fixed dimer, trimer, tetramer and pentamer geometries using the 6-311G** basis sets at the MP2 level of theory were all done using *CADPAC*. To investigate the effect of additional polarisation functions on the potential energy surface, the dimer calculation with the monomers at the crystallographic separation was repeated using the 6-311G basis set with functions 3d, 1f on the heavy atoms and 3s, 1p on the hydrogen atoms.

Counterpoise corrections were performed for the dimer calculations at each of the monomer separations for the 6-311G** basis set at both the SCF and MP2 levels of theory. In addition, the SCF and MP2 dimer calculations with the monomers at the crystallographic separation using the 6-311G basis set with

functions 3d, 1f on the heavy atoms and 3s, 1p on the hydrogen atoms were corrected for counterpoise.

2.3 Results and Discussion

2.3.1 Formamide

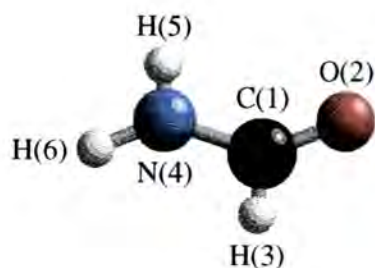


Figure 2.1 Formamide

The bond lengths and angles for formamide (the monomer unit of the larger systems) optimised at different levels of theory are shown in *table 2.1*. It can be seen that increasing the level of theory showed a decrease in energy for the same basis set, which is expected due to the inclusion of the electron correlation energies. For both the 6-31G* and 6-311G** basis sets, all the parameter values are lowered for the MP2 calculation relative to the SCF calculation, with the exception of $\angle O(2)C(1)H(3)$. Increasing the basis set for the different levels of theory also shows this trend, with the exception of $rC(1)-rH(3)$ and $rC(1)-rN(4)$. This is the case for all three basis sets.

The calculations carried out at the MP2 level showed the best agreement with the experimental data, and the 6-311G** basis set gave slightly better agreement than the 6-31G* basis for the parameters involving the hydrogen atoms. The final optimised geometry using the 6-311G** basis set at the MP2 level of theory was considered to be sufficiently accurate to use in the calculations on the hydrogen bonded complexes.¹⁶

Table 2.1 Optimised bond lengths and bond angles for formamide

Parameter	Basis set/level of theory					Expt [*]
	3-21G*/ SCF	6-31G*/ SCF	6-31G*/ MP2	6-311G**/ SCF	6-311G**/ MP2	
<i>Bond lengths</i>						
<i>r</i> C(1)— <i>r</i> O(2)	1.212	1.193	1.224	1.184	1.213	1.219
<i>r</i> C(1)— <i>r</i> H(3)	1.084	1.091	1.105	1.094	1.106	1.098
<i>r</i> C(1)— <i>r</i> N(4)	1.353	1.348	1.360	1.350	1.362	1.360
<i>r</i> N(4)— <i>r</i> H(5)	0.998	0.996	1.011	0.994	1.007	1.002
<i>r</i> N(4)— <i>r</i> H(6)	0.995	0.993	1.008	0.991	1.004	1.002
<i>Bond angles</i>						
<C(1)N(4)H(5)	119.426	119.289	118.913	119.250	118.886	118.8
<C(1)N(4)H(6)	121.939	121.811	121.880	121.447	121.446	121.4
<O(2)C(1)H(3)	122.420	122.335	122.900	122.278	123.144	122.7
<O(2)C(1)N(4)	125.310	124.954	124.748	125.134	124.991	124.5
<i>Energy</i>						
/kJ mol ⁻¹	-441044	-443528	-444774	-443664	-445186	-

All bond lengths in angstroms, all bond angles in degrees.

* Gas-phase spectroscopic data²²

2.3.2 The (methyl)acetamide dimer

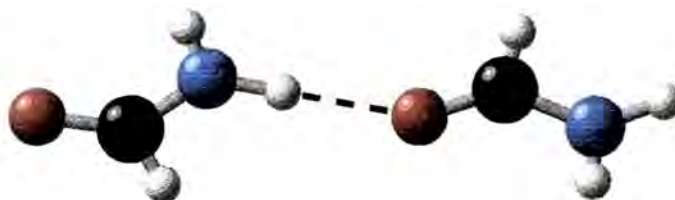


Figure 2.2 The (methyl)acetamide dimer

The potential energy curves for the dimer at different monomer separations are shown in *figures 2.3-2.8*. The effect of increasing the number of polarisation functions on the potential energy curve for the monomers at the equilibrium separation is shown in *figure 2.9*. The corresponding BSSE-corrected curves are also represented in *figures 2.3-2.9*, and plots of the stabilisation energy due to the basis set superposition effect against the N–H distance (the difference between the uncorrected and BSSE-corrected curves) are represented by *figures 2.10-2.16*. The parameter values for the potential energy curves (*cf. figure 1.1*) displaying double minima are given in *table 2.2*, and *figures 2.17-2.2* are graphical representations of these values.

General trends in the shape of the potential energy curves

The potential energy curve for the dimer with the monomers at the crystallographically defined separation (2.825 Å) has a single minimum for both the 6-311G** and 6-311G (3df, 3sp) basis sets at the SCF and MP2 levels of theory (*figures 2.3 and 2.9*). Increasing the monomer separation results in a double minimum for an increase of 0.4 Å at the SCF level, and for increases of 0.6 Å, 0.8 Å

and 1.0 Å for both the SCF and MP2 calculations (*figures 2.5-2.8*). The position of the first minimum is unchanged for all monomer separations, but as the separation is increased beyond 0.4 Å the position of the second monomer shifts to a larger N–H separation.

There are a number of possible reasons why a double minimum is not seen for the shorter N...O distances at either the SCF or MP2 levels. Discrepancies could arise because of the fact that the gas-phase monomer geometries have been placed relative to each other at the crystallographic separation and angle, and because the calculations were done on the fixed dimer geometry. The high *R* value of the crystal structure solution (17%)¹⁹ also suggests that there may be significant errors in the quoted crystallographic parameters.

Where a double minimum is observed, it can be seen that there are discrepancies between the energies calculated at the SCF level and at the MP2 level of theory. This error in the SCF potential surface is illustrated in *figure 2.5* for a monomer separation of 0.4 Å greater than the crystallographic separation, in which the calculation at the SCF level gives a potential energy surface with two minima but the MP2 level only shows one minimum on the potential curve. The potential energy surface is distorted along the proton transfer coordinate resulting in the formation of two distinct minima when in fact there is only one for this monomer separation, as shown in the electron correlated calculation.

There are a number of possible reasons for the inadequacies in the calculations at the SCF level. The first is BSSE, which in calculations on such systems can cause distortion of the potential energy surface in the manner described above. However, it can be seen from *figure 2.12* that the BSSE is sufficiently small (between 2 and 10 kJ mol⁻¹ along the N...O vector) to be discounted for leading to

the distortion of the potential energy curve at the SCF level. In fact, it can be seen from *figure 2.5* that the BSSE makes no difference to the general shape of the curve, and a double minimum still exists for the counterpoise-corrected energy surface.

Clearly, there must be another effect of a greater magnitude that results in such a dramatic difference between the Hartree-Fock and electron correlated potential energy surfaces at all the monomer separations. This could be due to the dissociation effect, a well-documented phenomenon that results in the closed-shell or restricted Hartree-Fock solution failing to adequately describe the dissociation of the molecular orbitals. The solution of the HF approximation then corresponds to a saddle point on the potential energy surface rather than a true minimum.

The remedy for this effect is generally considered to be an open-shell or unrestricted treatment.¹ It can be seen that for *figures 2.7* and *2.8* there are no counterpoise data available for the longest N–H separations which would correspond to the dissociation of the N–H bond. The lack of data is a consequence of the monomer calculations failing to converge at the SCF level for these ‘bond’ lengths. In an attempt to resolve this unrestricted HF methods were attempted in these cases, but it was still not possible to achieve SCF convergence. A likely explanation could be spin contamination (this should be no more than 10% to solve for an unrestricted solution) which has been a cause for much criticism of the simple UHF approach.¹

The failure of the unrestricted approach indicates a serious breakdown of the Hartree-Fock approximation, and suggests that it would perhaps be necessary to use multiconfiguration methods¹ to obtain a solution for these monomer energies. There is much scope for investigation of this particular problem. For the purpose of this investigation, it can be seen that the unavailable data are located at the steepest

gradient of the potential well, and the double minima are present in both the counterpoise-corrected and the uncorrected energy surfaces.

It is clear from these findings that the SCF energies in *all* the dimer cases must be treated with suspicion, as the fact that the SCF calculations break down at a certain monomer and N–H separation indicates an inadequate description of the electronic effects present at this level of theory. This corroborates previous conclusions that “...*Hartree-Fock calculations should not be used if reliable...potential energy surfaces for hydrogen bonded systems are needed...*”¹⁶

Indeed, it is also possible that the electron correlation level of theory used is insufficient, although it is generally considered that calculations at the MP2 level are satisfactory when applied with adequate basis sets for investigating such a process.¹² The results of the counterpoise correction for the MP2 data suggest that this is in fact the case, and are discussed below.

Counterpoise-corrected data

The effect of increasing the monomer separation on the stabilisation energy brought about by BSSE is illustrated in *figures 2.10-2.16*. The stabilisation energy increases as the N–H distance is increased, and the rate of increase at the MP2 level can be seen to be approximately three times that at the SCF. This is expected, as corrections for correlated wavefunctions are generally larger than for SCF. The dependence of the BSSE on the distance could indicate that the interaction between monomers at a given separation is dominated by dispersion (a long-range attractive force resulting from the correlation of the motions of the electrons in two molecules) which is often the case in hydrogen bonded complexes.¹⁴

It has been noted that “*in [such] cases there would be little point in removing the BSSE by applying the counterpoise recipe, since the errors remaining after such correction would still be very large*”.¹⁴ The only solution for this state of affairs is to carry out well-correlated calculations using large customised basis sets including diffuse functions to minimise BSSE. Some researchers have suggested using 6-311++G(3d, 3p) basis sets at the MP3 level,²³ but electron correlation at MP2 is probably sufficient for most purposes.

The relatively small stabilisation energies (between 2 and 10 kJ mol⁻¹ at the SCF level, 5 and 35 kJ mol⁻¹ at the MP2) and the increase in these energies with N–H distance point to the unreliability of the counterpoise procedure in correcting for BSSE in this instance. This is illustrated by comparing the results of the calculations using the 6-311G** basis set and the 6-311G(3df, 3sp) basis sets for the monomers at the crystallographic separation (*figures 2.10 and 2.16* respectively). The difference in the magnitude of the stabilisation energy is significantly higher for the SCF calculation (between 39 and 43 kJ mol⁻¹), although for the MP2 calculation it is of a similar value for a given N–H separation.

This large discrepancy in the values for the SCF calculation suggest that the 6-311G** basis set is inadequate for a study of such a system, as improving the basis set should reduce the BSSE. In this case, the stabilisation energy *increases* for a larger basis set. Clearly, the corrections for the larger basis set are more certain than those for the smaller, and as the magnitude of the counterpoise correction is generally regarded as a guide to the reliability of the result, it must be concluded that BSSE is a significant problem even for the larger basis set. Only by improving the basis set beyond 6-311G**(3df, 3sp) would one see a decrease in the correction and a subsequent improvement in the result.

The consistency of the size of the stabilisation energy at the MP2 level for the two basis sets suggests that this level of theory is sufficient to describe electron correlation for a given basis set.

Effect of the monomer separation and electron correlation on the shape of the curves

The parameters for the potential curves exhibiting double minima are presented in *table 2.2*. These parameter values were obtained simply by subtracting the minima positions and energies from each other. Although the data from the SCF calculations are also included for comparison, from the discussion above it must be concluded that this level of theory is insufficient to describe electronic effects in the (methyl)acetamide dimer.

Increasing the monomer separation results in the increase of the potential surface parameters for the double minima (*figure 1.1*), that is, the minima separation (Δr), the energy difference between them (ΔE) and the activation energy barrier (E_a) for the process. This suggests that there is an optimum N...O distance for proton transfer, and the present results indicate this value to be 3.2 – 3.4 Å which is unfeasible for this system on the basis of the vibrational spectroscopic results.²⁴

The increase in the monomer separation with the parameter values for the double minimum potential energy curve is linear (*figures 2.17-2.19*). This implies that there are no energetic changes that are unaccounted for as the monomer separation is increased, allowing a direct comparison to be made of the results for the different monomer separations.

Figures 2.20 and 2.21 show the change in energy difference between the minima and activation energy (ΔE and E_a respectively) with the change in the

minima separation, Δr . These are both linear relationships for the SCF and MP2 energies, but while there is negligible difference in the gradient for the SCF and MP2 cases for the change in ΔE , the gradient for the SCF energy for the plot against E_a is significantly steeper than that for the MP2 energy.

This can be attributed to the fact that at the SCF level the activation energy is over-estimated compared to that for the MP2 level for a given monomer separation due to BSSE, and that this error increases with the monomer separation.¹⁶ There is no difference in the gradient for the plot against ΔE because the energy difference between the minima is a relative property of the potential surface, with the error in the SCF calculation present in the values for Δr (*figure 2.19*).

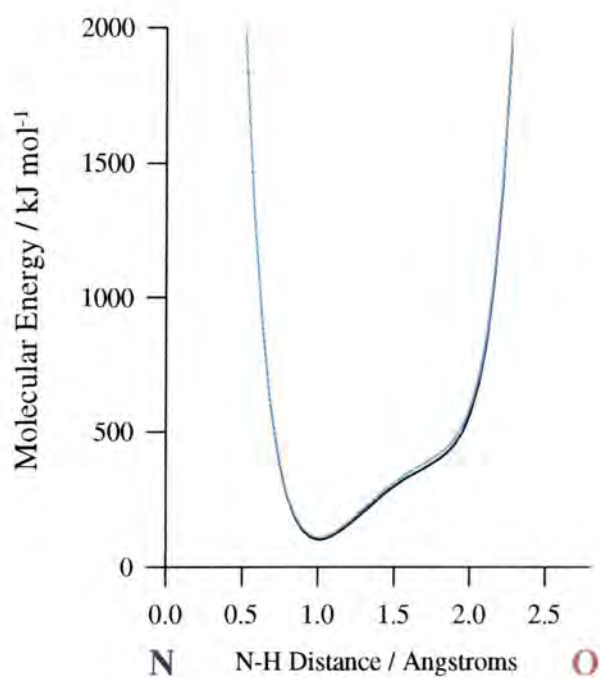
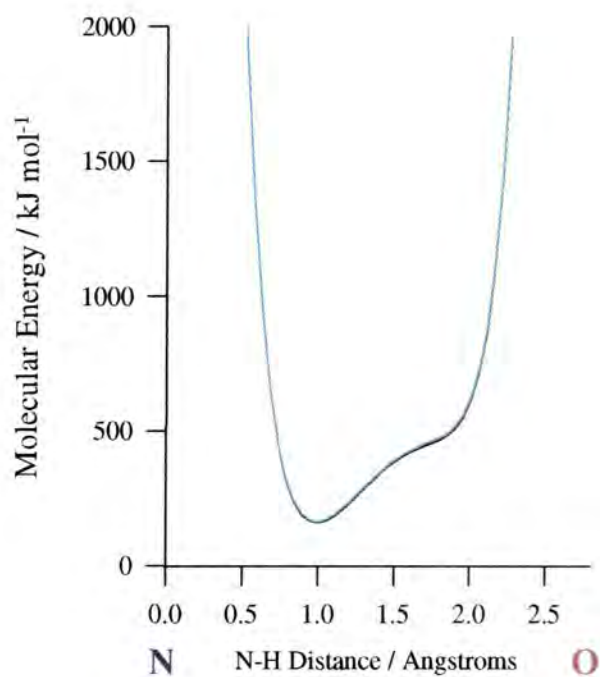


Figure 2.3 Potential energy curve (6-311G** basis set/SCF energy top, MP2 energy bottom) for the (methyl)acetamide dimer, with the monomer units at the crystallographically defined separation. The BSSE-corrected curve is shown in blue.

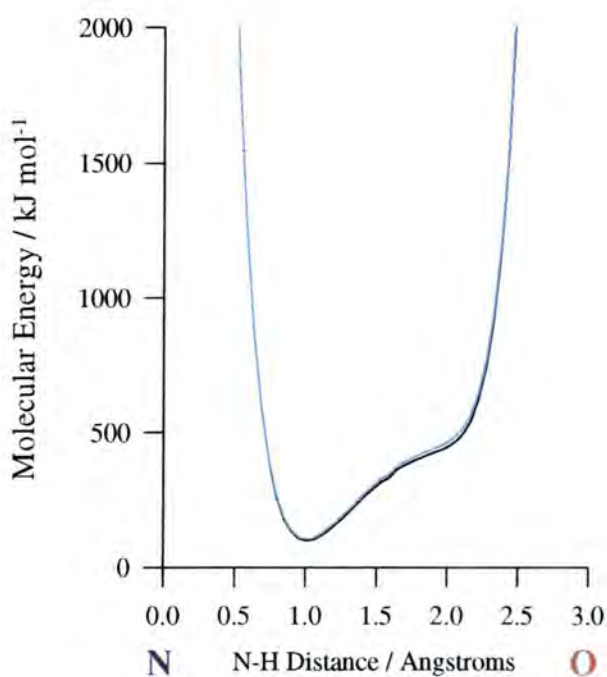
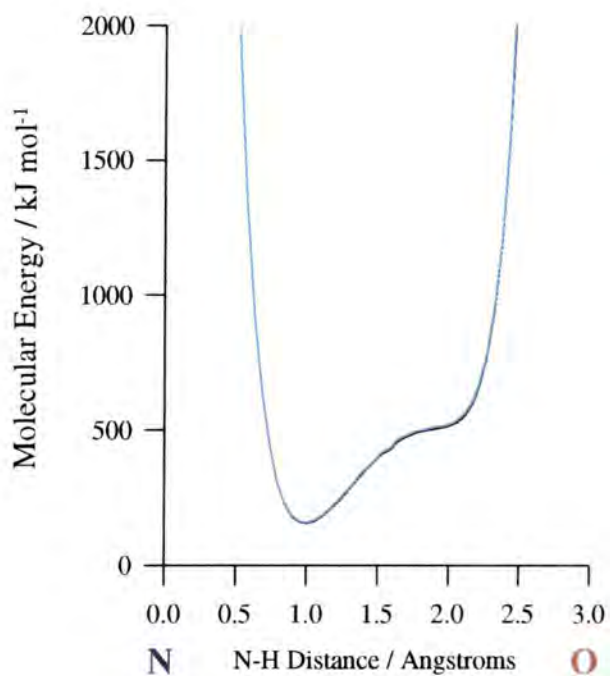


Figure 2.4 Potential energy curve (6-311G** basis set/SCF energy top, MP2 energy bottom) for the (methyl)acetamide dimer, with the separation between the monomer units increased by 0.2 Å. The BSSE-corrected curve is shown in blue.

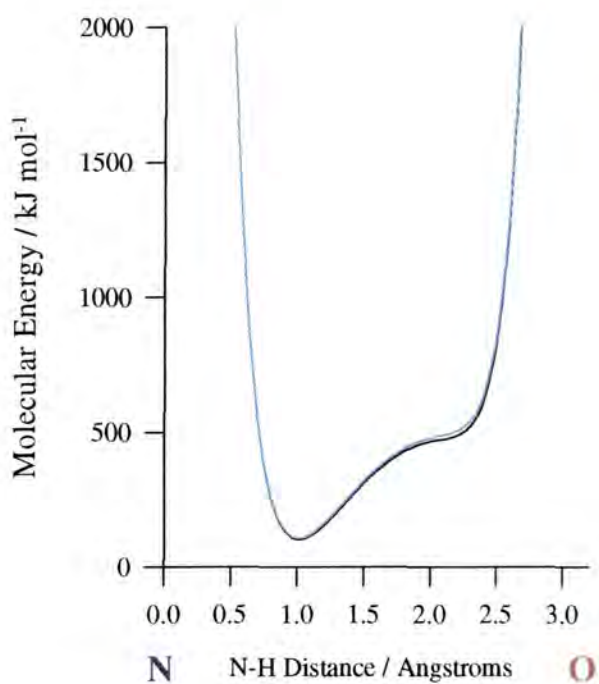
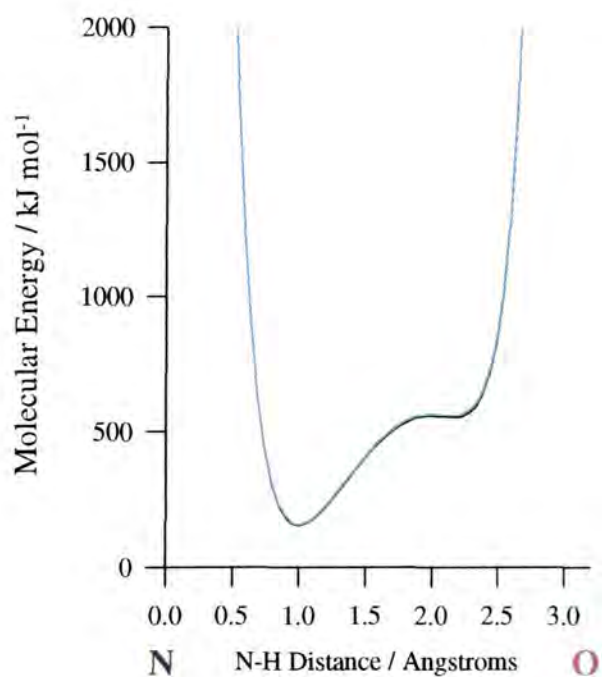


Figure 2.5 Potential energy curve (6-311G** basis set/SCF energy top, MP2 energy bottom) for the (methyl)acetamide dimer, with the separation between the monomer units increased by 0.4 Å. The BSSE-corrected curve is shown in blue.

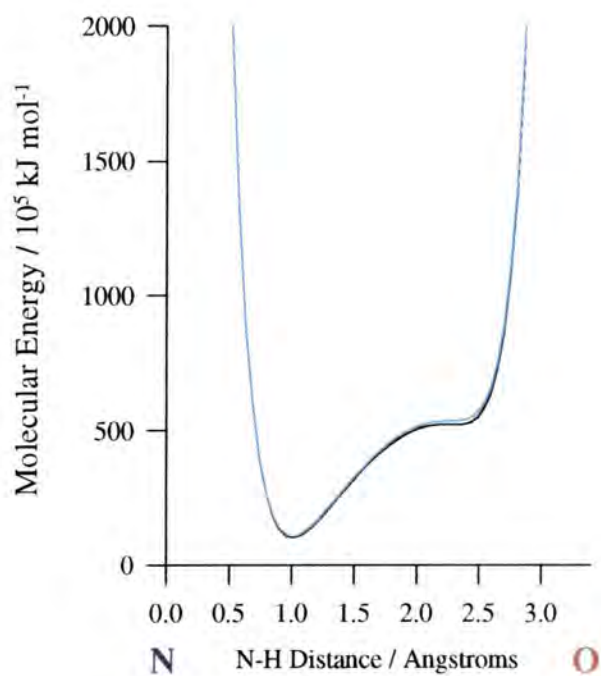
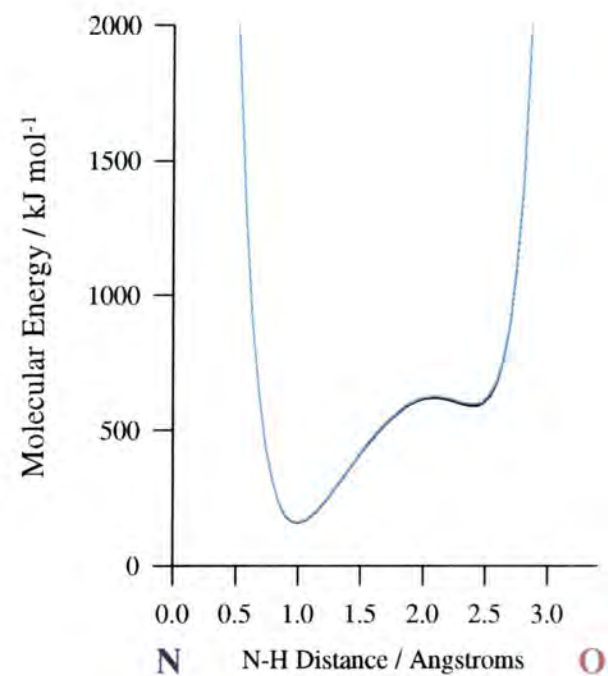


Figure 2.6 Potential energy curve (6-311G** basis set/SCF energy top, MP2 energy bottom) for the (methyl)acetamide dimer, with the separation between the monomer units increased by 0.6 Å. The BSSE-corrected curve is shown in blue.

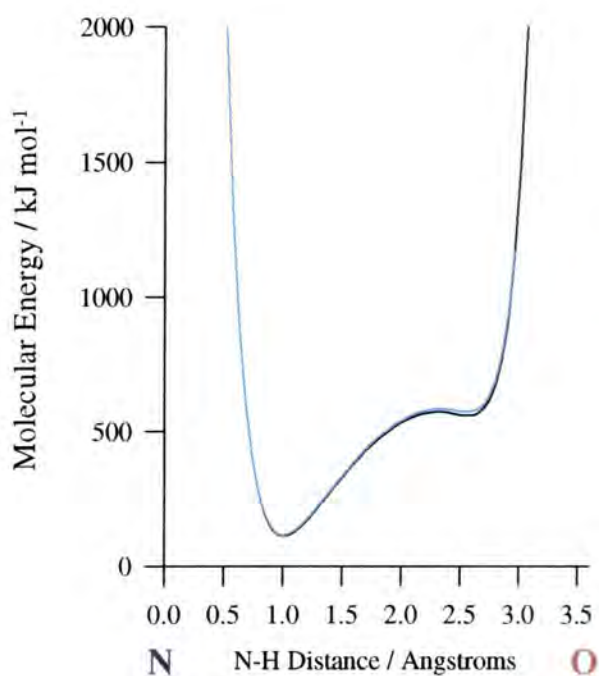
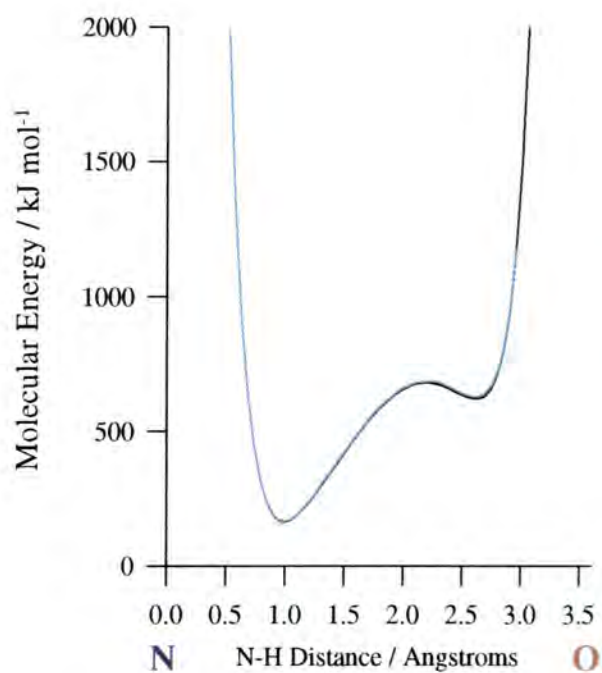


Figure 2.7 Potential energy curve (6-311G** basis set/SCF energy top, MP2 energy bottom) for the (methyl)acetamide dimer, with the separation between the monomer units increased by 0.8 Å. The BSSE-corrected curve is shown in blue.

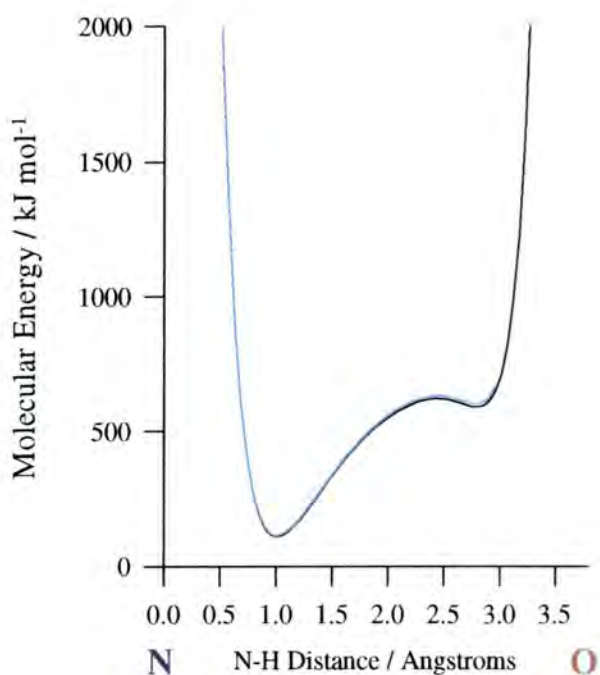
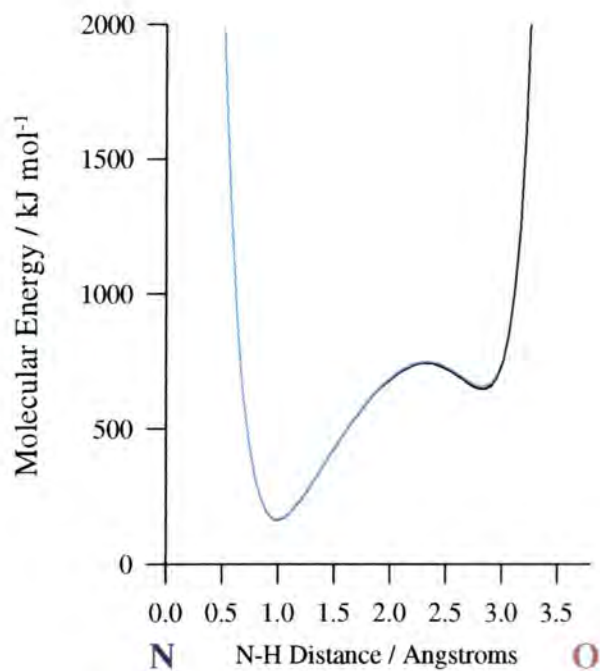


Figure 2.8 Potential energy curve (6-311G** basis set/SCF energy top, MP2 energy bottom) for the (methyl)acetamide dimer, with the separation between the monomer units increased by 1.0 Å. The BSSE-corrected curve is shown in blue.

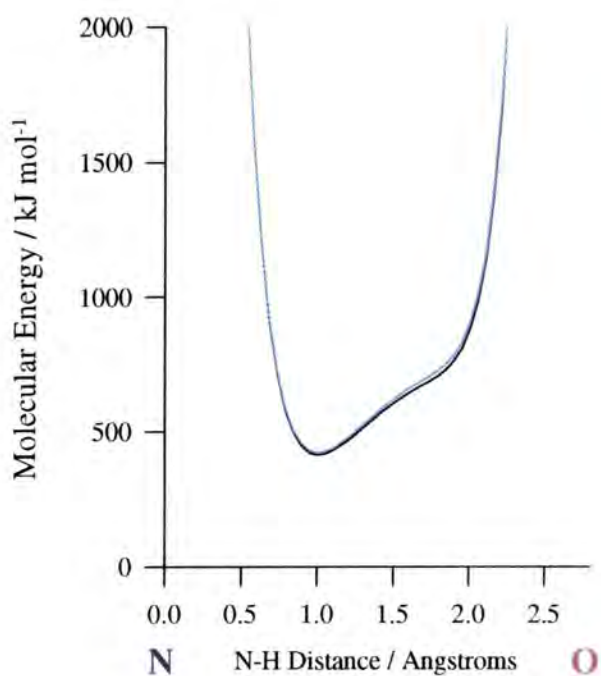
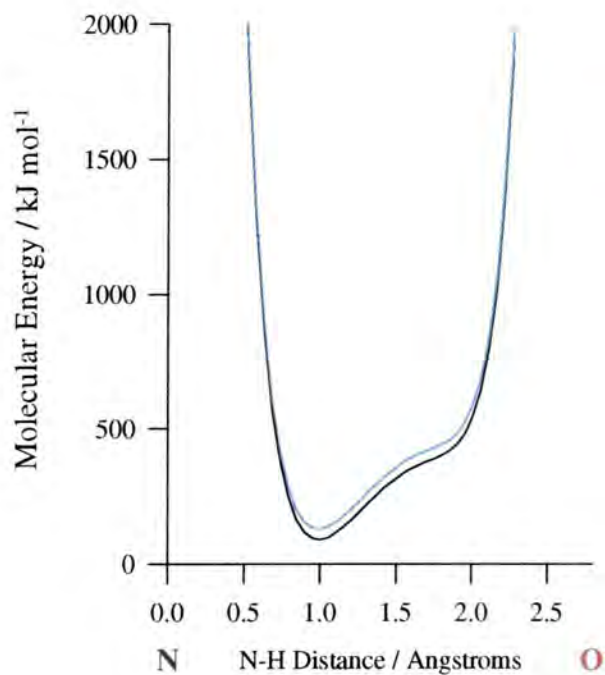


Figure 2.9 Potential energy curve (6-311G (3df, 3sp) basis set/SCF energy top, MP2 energy bottom) for the (methyl)acetamide dimer, with the monomer units at the crystallographically defined separation. The BSSE-corrected curve is shown in blue.

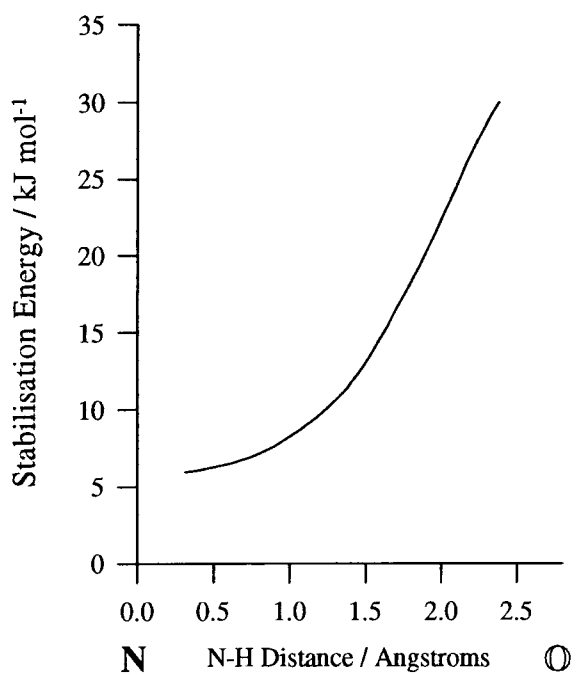
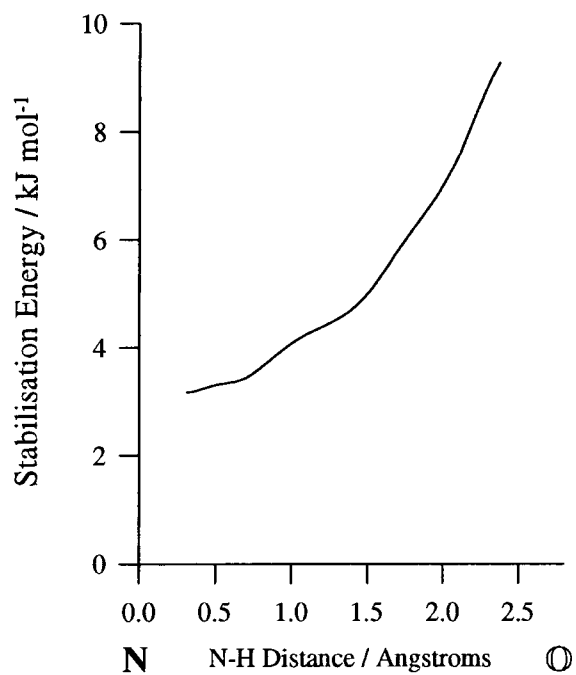


Figure 2.10 Stabilisation energy due to BSSE for the (methyl)acetamide dimer (6-311G** basis set/SCF top, MP2 bottom), with the monomer units at the crystallographic separation.

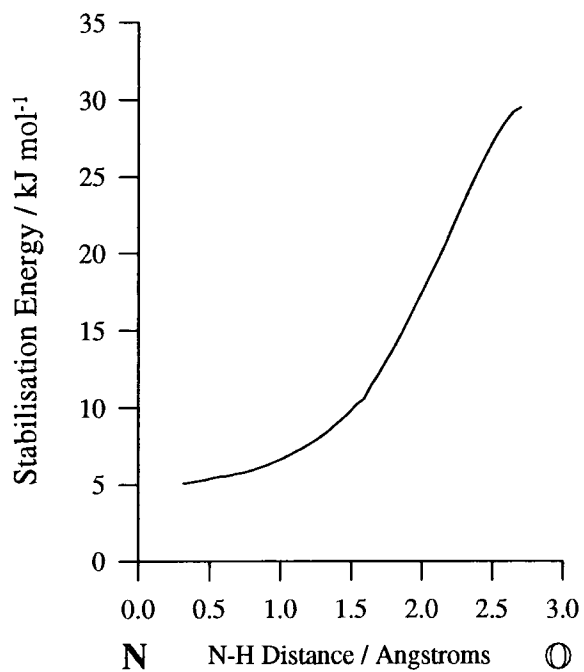
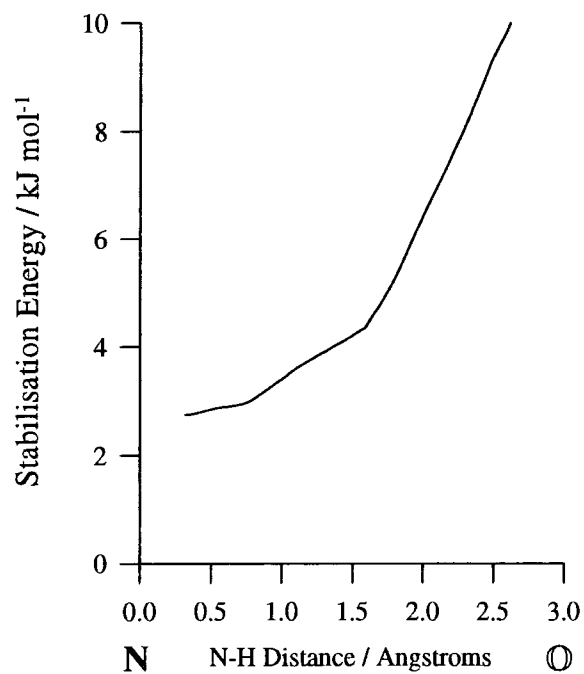


Figure 2.11 Stabilisation energy due to BSSE for the (methyl)acetamide dimer (6-311G** basis set/SCF top, MP2 bottom), with the separation between the monomer units increased by 0.2 Å.

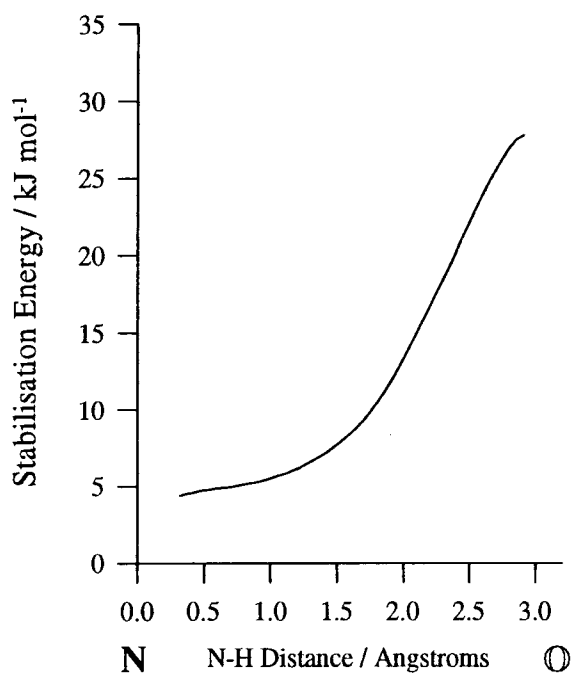
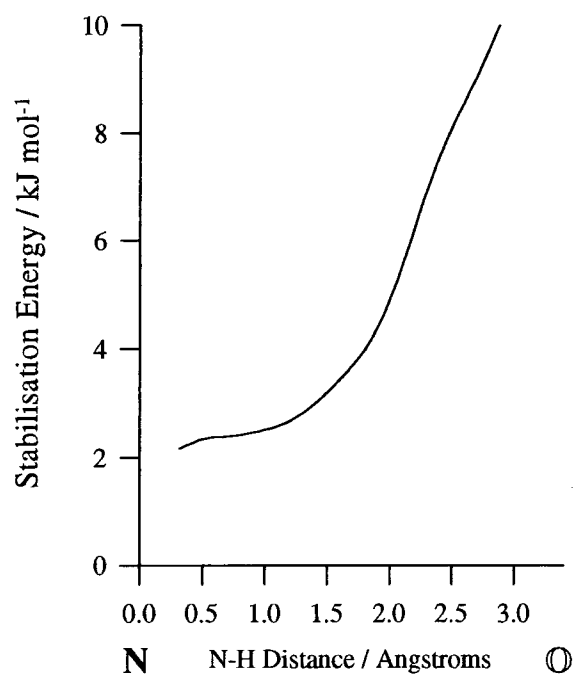


Figure 2.12 Stabilisation energy due to BSSE for the (methyl)acetamide dimer (6-311G** basis set/SCF top, MP2 bottom), with the separation between the monomer units increased by 0.4 Å.

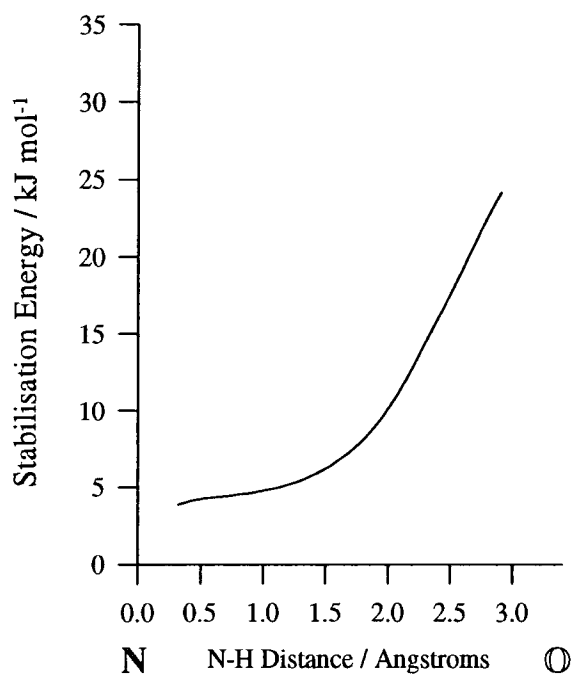
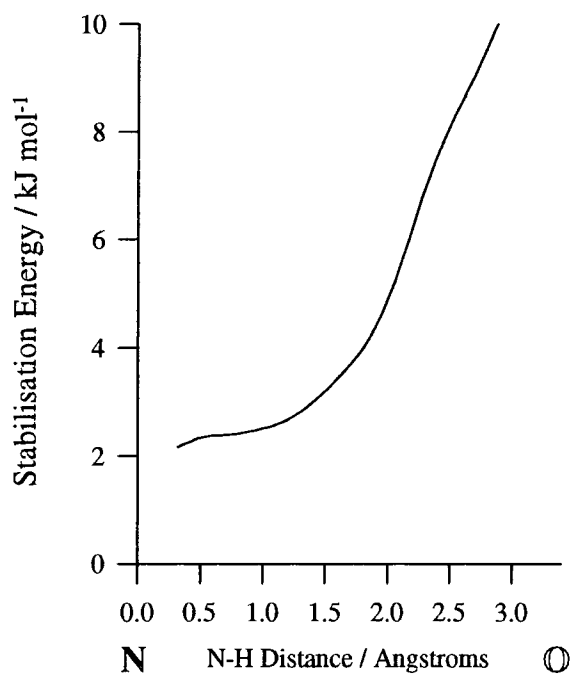


Figure 2.13 Stabilisation energy due to BSSE for the (methyl)acetamide dimer (6-311G** basis set/SCF top, MP2 bottom), with the separation between the monomer units increased by 0.6 Å.

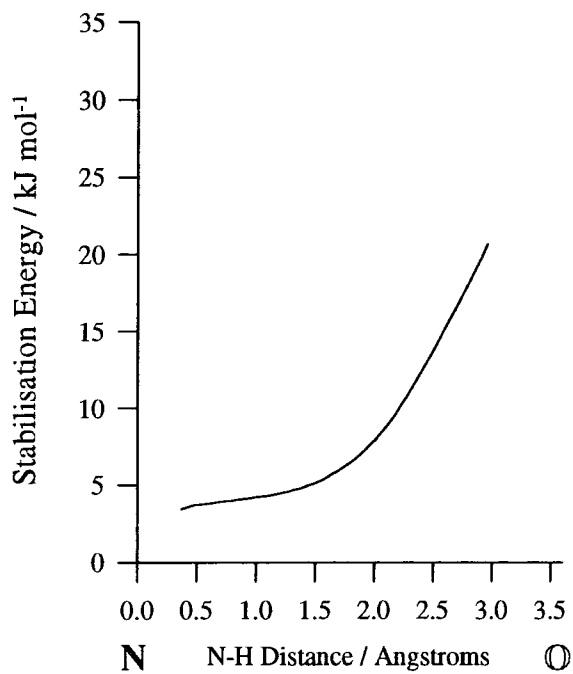
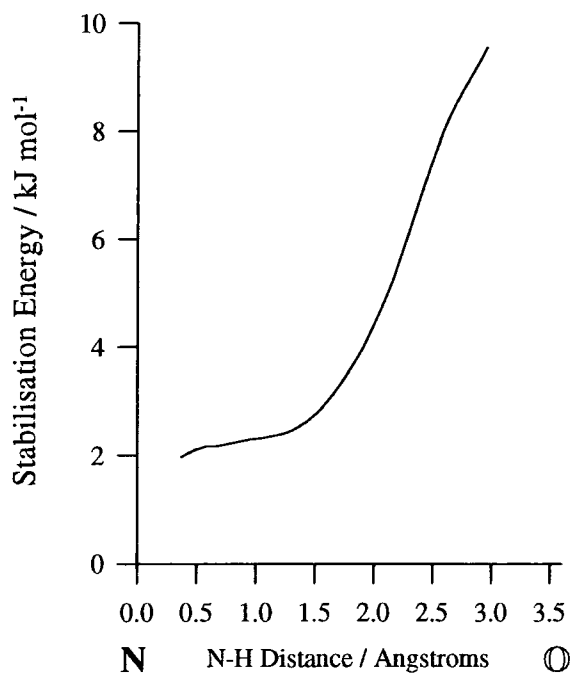


Figure 2.14 Stabilisation energy due to BSSE for the (methyl)acetamide dimer (6-311G** basis set/SCF top, MP2 bottom), with the separation between the monomer units increased by 0.8 Å.

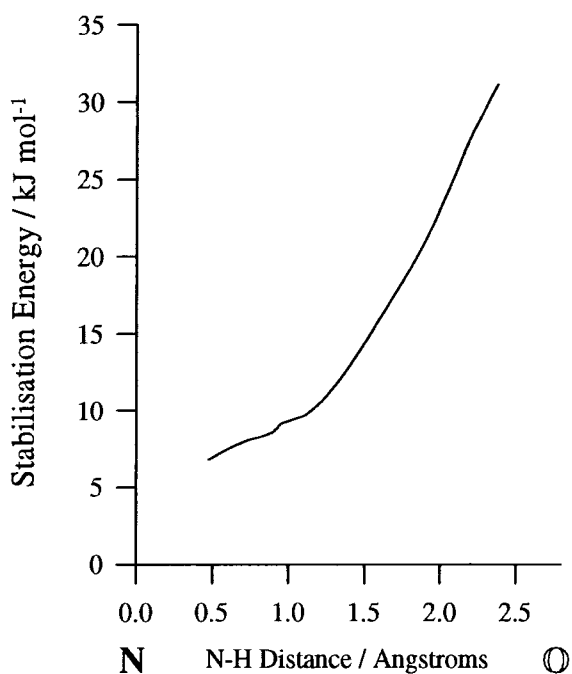
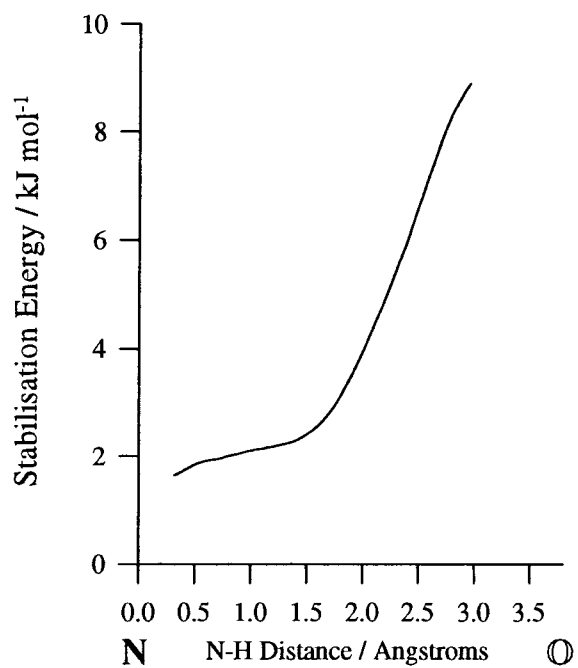


Figure 2.15 Stabilisation energy due to BSSE for the (methyl)acetamide dimer (6-311G** basis set/SCF top, MP2 bottom), with the separation between the monomer units increased by 1.0 Å.

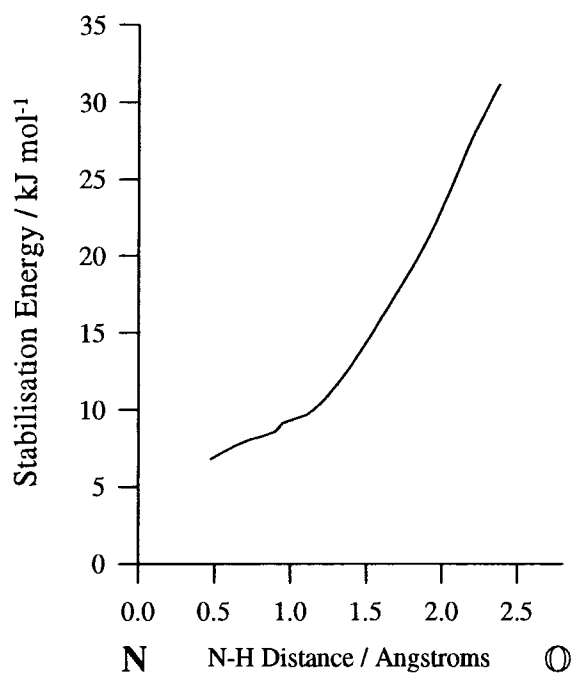
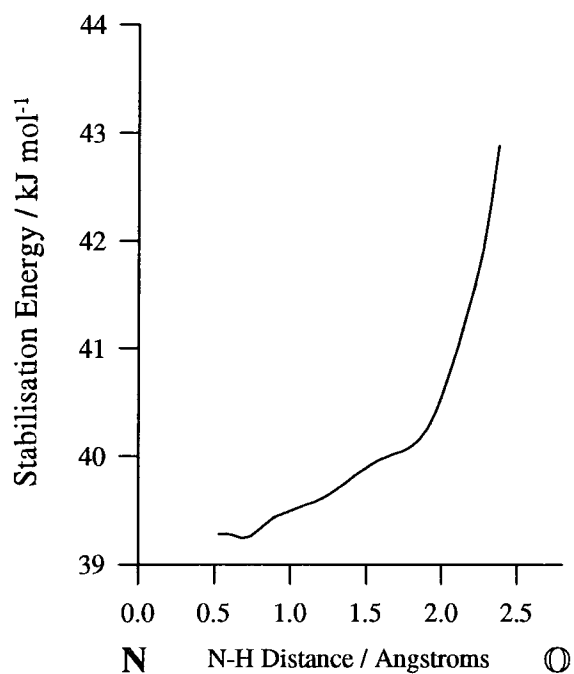


Figure 2.16 Stabilisation energy due to BSSE for the (methyl)acetamide dimer (6-311G (3df, 3sp basis/SCF top, MP2 bottom), with monomer units at the crystallographic separation.

Table 2.2 Parameters for the calculated potential energy curves of the (methyl)acetamide dimer at different monomer separations, using the 6-311G** basis set at the SCF and MP2 levels of theory

Parameter	Increase in monomer separation from the crystallographically defined value (Å) / level of theory of calculation						
	0.4		0.6		0.8		1.0
	SCF	SCF	MP2	SCF	MP2	SCF	MP2
E_a / kJ mol ⁻¹	401.078	460.650	418.308	518.372	463.119	580.011	513.343
ΔE / kJ mol ⁻¹	396.007	430.910	417.689	456.872	448.194	483.742	479.566
Δr / Å	1.16	1.38	1.32	1.64	1.59	1.85	1.80

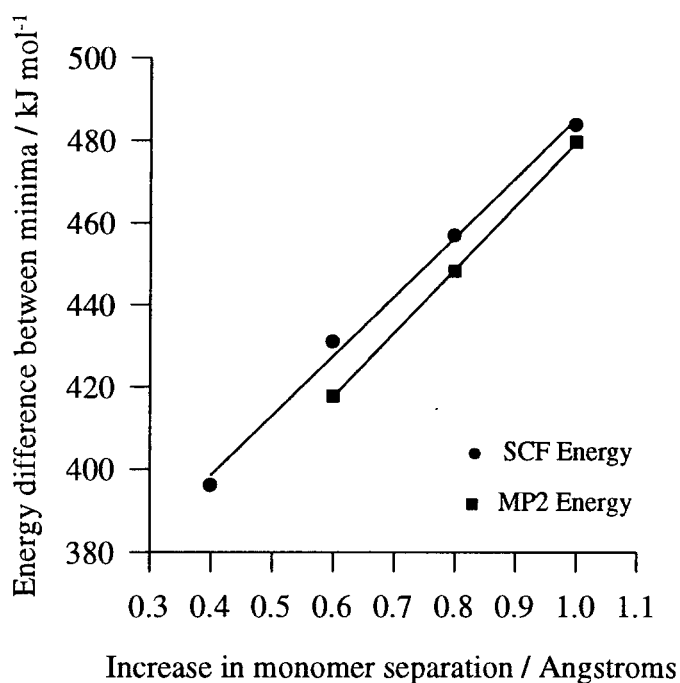


Figure 2.17 Change in energy difference between minima (ΔE) with increase in monomer separation.

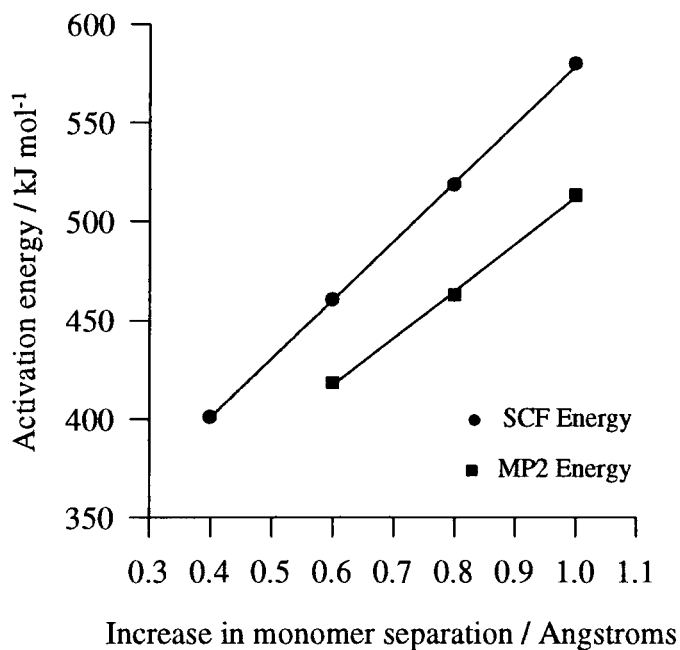


Figure 2.18 Change in activation energy (E_a) with increase in monomer separation.

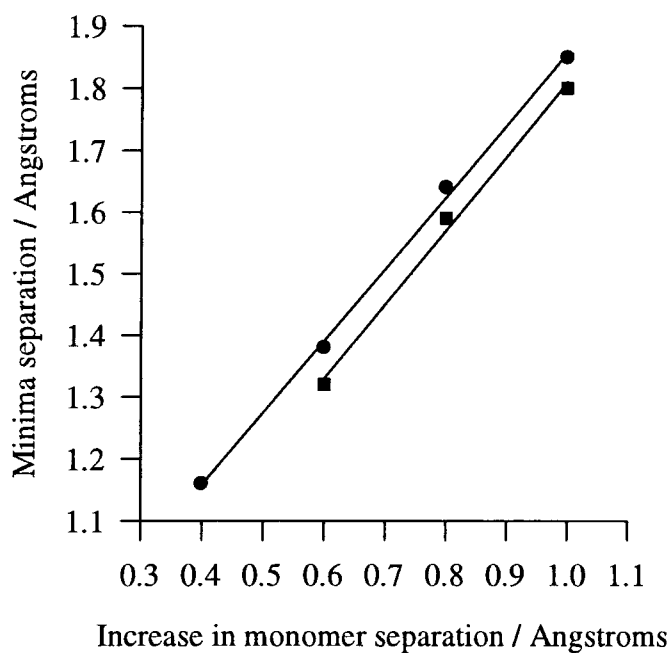


Figure 2.19 Change in minima separation (Δr) with increase in monomer separation.

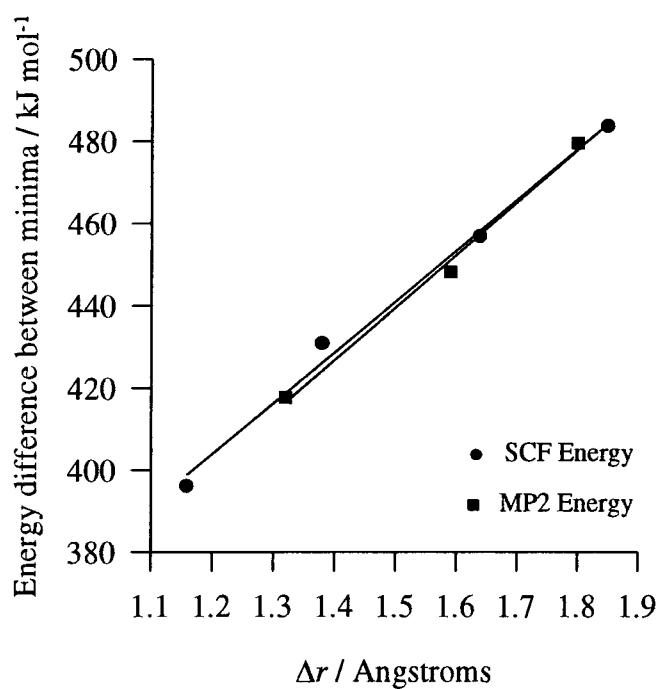


Figure 2.20 Change in energy difference between minima (ΔE) with difference in minima separation (Δr).

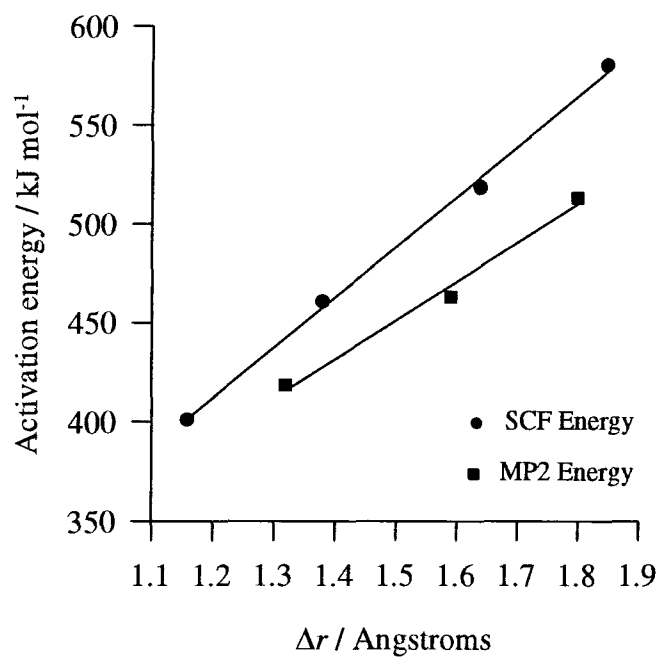


Figure 2.21 Change in activation energy (E_a) with difference in minima separation (Δr).

2.3.3 The (methyl)acetamide trimer



Figure 2.22 The (methyl)acetamide trimer

Figure 2.23 shows the results of SCF and MP2 calculations on the (methyl)acetamide trimer. At both levels the curves show a single minimum on the potential energy surface, although they differ from those obtained for the dimer at the crystallographic separation in having a more pronounced ‘shoulder’.

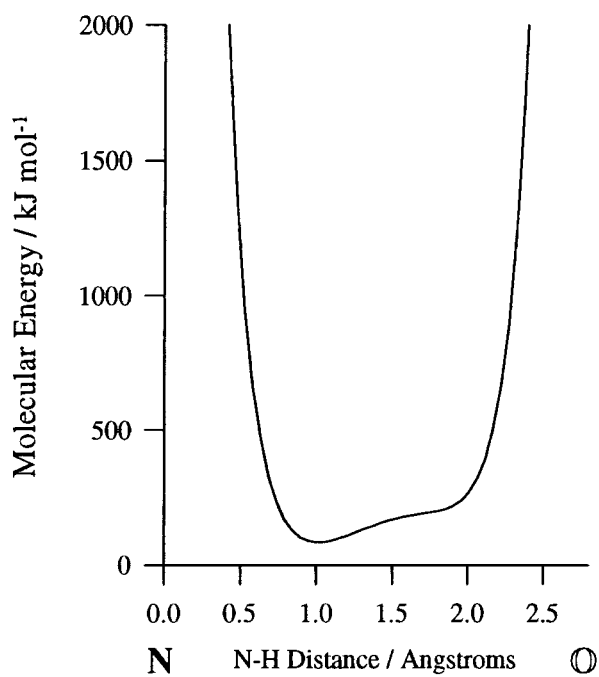
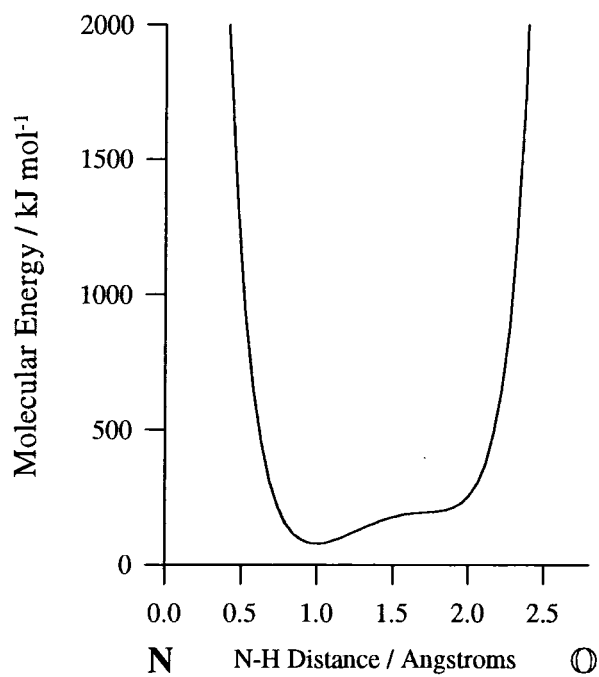


Figure 2.23 Potential energy curve (6-311G basis set/SCF energy top, MP2 energy bottom) for the (methyl)acetamide trimer, with the monomer units at the crystallographically defined separation.

2.24 The (methyl)acetamide tetramer

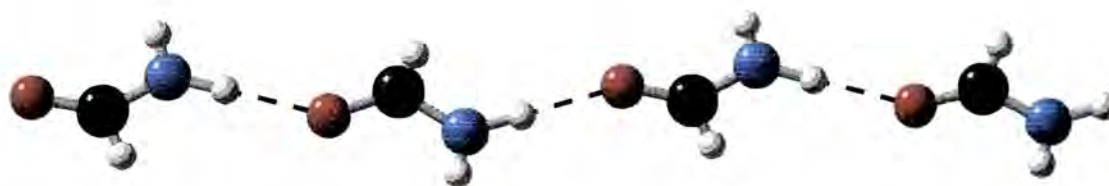


Figure 2.24 The (methyl)acetamide tetramer

Figure 2.25 shows the results of SCF and MP2 calculations on the (methyl)acetamide tetramer. The shapes of the curves are similar to those obtained for the trimer, but with more enhanced features relative to the dimer potential surfaces for the same monomer separation.

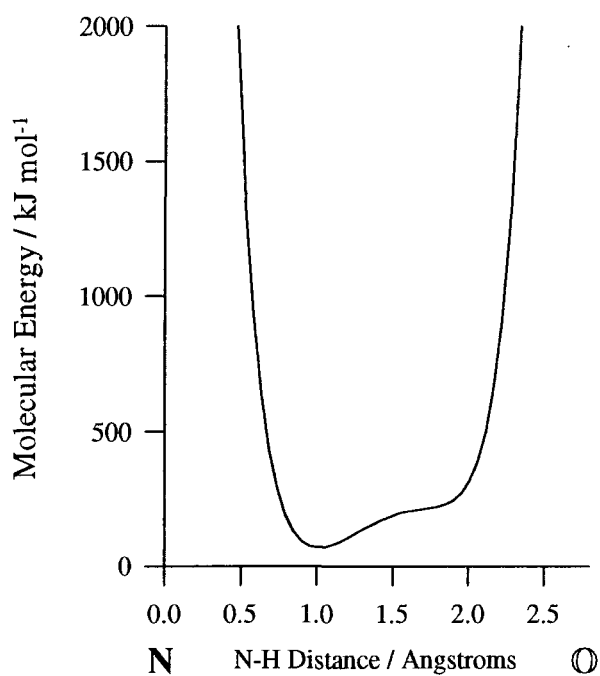
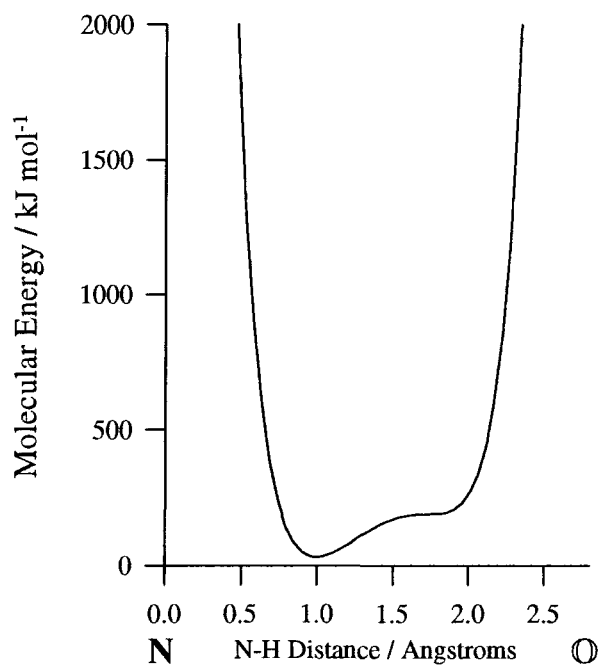


Figure 2.25 Potential energy curves (6-311G basis set/SCF energy top, MP2 energy bottom) for the (methyl)acetamide tetramer, with the monomer units at the crystallographically defined separation.

2.2.5 The (methyl)acetamide pentamer



Figure 2.26 The (methyl)acetamide pentamer

Figure 2.27 shows the results of SCF and MP2 calculations on the (methyl)acetamide tetramer. At the SCF level, the potential curve is a double minimum, and the parameters for the curve are displayed in *table 2.3*. The curve obtained at the MP2 level only exhibits a single potential, and it must be concluded that the double minimum obtained at the SCF level is due to the distortion of the potential surface owing to a breakdown of the RHF approximation at certain N–H separations. The parameter values thus obtained must therefore be considered to be unreliable. In any case, it is not possible to draw any direct quantitative comparisons between the results for this system and the dimer.

However, the fact that a double minimum is obtained, even at the SCF level, is an interesting result. The MP2 curve shows a more defined shoulder relative to the trimer and tetramer calculations, and suggests that increasing the number of monomer units further may result in a double minimum at the crystallographically defined separation.

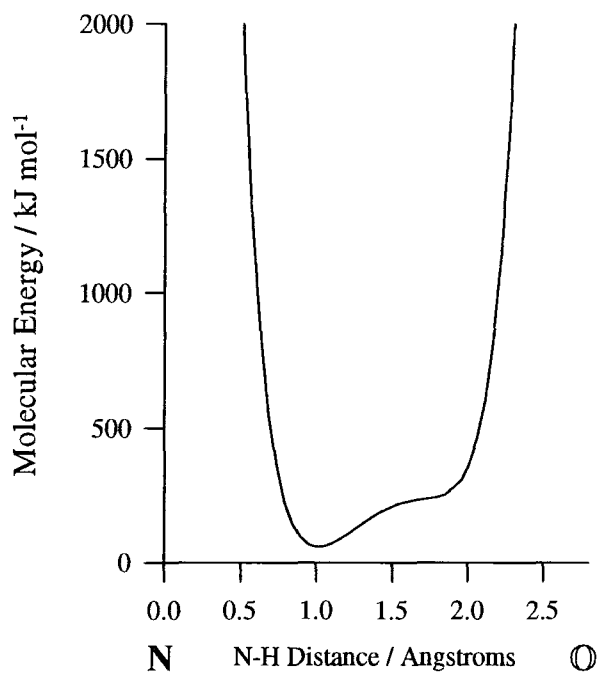
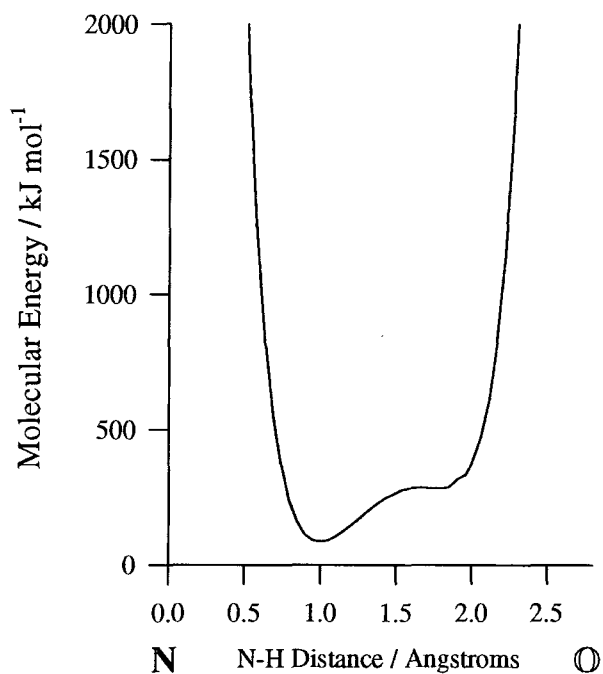


Figure 2.27 Potential energy curves (6-311G basis set/SCF energy top, MP2 energy bottom) for the (methyl)acetamide pentamer, with the monomer units at the crystallographically defined separation.

Table 2.3 Parameters for the calculated potential energy curve of the (methyl)acetamide pentamer using the 6-311G** basis set at the SCF level of theory

Parameter	Parameter values for the (methyl)acetamide pentamer
$E_a / \text{kJ mol}^{-1}$	831.147
$\Delta E / \text{kJ mol}^{-1}$	825.775
$\Delta r / \text{\AA}$	0.79

2.4 References

- [1] R. McWeeny, “*Methods of Molecular Quantum Mechanics*”, chapters 1 and 6, (Academic Press, 1992)
- [2] J. B. Foresman and Æleen Frisch, “*Exploring Chemistry with Electronic Structure Methods*”, Appendix A, (Gaussian Inc., 1996)
- [3] N. C. Handy, *Laredo Quantum Chemistry School Lecture Notes* (1994)
- [4] A. Hinchcliffe, “*Computational Quantum Chemistry*”, chapter 2, (Wiley, 1989)
- [5] I. N. Levine, “*Quantum Chemistry*”, chapters 6 and 11, (Prentice Hall, 1991)
- [6] K ello, V., Sadlej, A. J. *Theor. Chim. Acta* **81**, 339, (1992)
- [7] Sadlej, A. J. *Theor. Chim. Acta* **79**, 123, (1991)
- [8] Sadlej, A. J. *Theor. Chim. Acta* **80**, 7, (1992)
- [9] Bearpark, M. J., Handy, N. C. *Theor. Chim. Acta* **84**, 115, (1991)
- [10] Frisch, M. J., Pople, J. A., Binkley, J. S. *J. Chem. Phys.* **80**, 7, (1984)
- [11] Chalasinski, G., Szczesniak, M. M. *Chem. Rev.* **94**, 1723, (1994)
- [12] F. B. van Duijneveldt, ‘Basis set superposition error’ in “*Molecular Interactions: From van der Waals to Strongly Bound Complexes*” ed. S. Scheiner, (Wiley, 1997)
- [13] Boys, S. F., Bernardi, F. *Molec. Phys.* **19**, 553, (1970)
- [14] A. J. Stone, “*The Theory of Intermolecular Forces*”, chapter 5, (Clarendon Press, 1996)
- [15] Gutowski, M., van Duijneveldt-van de Rijdt, J. G. C. M., van Lenthe, J. G. and van Duijneveldt, F. B. *J. Chem. Phys.* **98**, 4728, (1993)

- [16] J. E. DelBene and I. Shavitt, 'The quest for reliability in calculated properties of hydrogen-bonded complexes' in "*Molecular Interactions: From van der Waals to Strongly Bound Complexes*" ed. S. Scheiner, (Wiley, 1997)
- [17] Kohn, W., Becke, A. D., Parr, R. G. *J. Phys. Chem.* **100**, (31), 12974, (1996)
- [18] A. J. Stone, "*The Theory of Intermolecular Forces*", chapter 5, (Clarendon Press, 1996)
- [19] Katz, J. L., Post, B. *Acta Cryst.* **13**, 624, (1960)
- [20] GAMESS (*General Atomic and Molecular Electronic Structure System*) Schmidt, M. W., Baldridge, K. K., Boatz, J. A., Elbert, S. T., Gordon, M. S., Jensen, J. W., Koseki, S., Matsunaga, N., Nguyen, K. A., Su, S. J., Windus, T. L., Dupuis, M., Montgomery, J. A. *J. Comp. Chem.* **14**, (11), 1347, (1993)
- [21] CADPAC (*The Cambridge Analytical Data Package, Issue 6, University of Cambridge, Cambridge, UK*) Amos, R. D., (1994)
- [22] Brown, R. D., Godfrey, P. D., Kleibomer, B. J. *J. Mol. Struct.* **124**, 34, (1987)
- [23] Yin, D., MacKerell, D. *J. Phys. Chem.*, **100**, 2588, (1996)
- [24] Kearley, G. J., Fillaux, F., Baron, M.-H., Bennington, S., Tomkinson, J. *Science* **264**, 1285, (1994)

CHAPTER 3

Distributed Multipole

Electrostatic Models

3.1 Theory

3.1.1 The electrostatic potential

Intermolecular forces can be divided into those having long-range and those having short-range effects. Long-range forces are the induction energy, dispersion energy and the electrostatic potential, and short-range forces are charge transfer and exchange-repulsion energy.¹ In considering an interaction such as hydrogen bonding between molecules, electrostatic forces are the most important as they determine the orientation dependence of the total intermolecular potential.²

The electrostatic potential is defined as the “*Coulombic interaction between the charge distributions of the molecules when they have not been distorted by the interaction*”,² and can be represented as follows:

$$U_{\text{static}} = \int_{\text{allspace}} \frac{\rho^A(\mathbf{r}_1)\rho^B(\mathbf{r}_2)}{4\pi\epsilon_0|\mathbf{r}_1 - \mathbf{r}_2|} d^3\mathbf{r}_1 d^3\mathbf{r}_2 = \langle 0^A 0^B | H' | 0^A 0^B \rangle \quad (3.1)$$

where H' is the perturbation operator equal to $\sum \frac{e_i e_j}{(4\pi\epsilon_0 r_{ij})}$,

ρ^A is the charge distribution corresponding to the ground-state wavefunction 0^A of a molecule A in isolation,

ρ^B is the charge distribution corresponding to the ground-state wavefunction 0^B of a molecule B in isolation.²

The electrostatic potential can be calculated from the wavefunctions of molecules that are obtained from *ab initio* calculations.

3.1.2 Distributed multipole models of the electrostatic potential

Calculation of the electrostatic potential has traditionally been done by using a central multipole expansion (for small molecules) or by using an atomic point charge model. This is because it is necessary to use an analytical procedure to express the electrostatic energy as a function of the relative orientations of two molecules (or a molecule and a point charge ‘probe’) due to the large number of possible relative orientations.

An alternative to these methods is to use the distributed multipole analysis (DMA).^{3,4} This technique uses not only point charges (as in an atomic point charge model) but point dipoles, quadrupoles, hexadecapoles *etc.* to represent the charge distribution around molecules.²⁻⁵ It has the advantage over the central multipole expansion technique of being applicable to markedly non-spherical molecules and there are not the convergence problems at shorter molecular separations as with the central multipole expansion. DMA has been described as “*a more complete alternative*”² to central multipole expansion and the point charge model as it is, in effect, the union of the other two methods.

The basis of DMA rests on distributing multipole centres around the molecules to give a model of the molecular potentials. The technique is based on the density matrix of the molecule, which can be expressed as follows (*equation 3.2*),

$$\rho(r) = \sum_{ij} \rho_{ij} \phi_i \phi_j \quad (3.2)$$

where ϕ_i, ϕ_j are Gaussian primitives comprising the atomic orbital set.

The origin and exponents of the Gaussian primitives represent the charge density at a series of point multipoles – charges, dipoles, quadrupoles, hexadecapoles *etc.* For two *s* orbitals, the charge density overlap is described by a charge and a

dipole, for two p orbitals by a charge, a dipole and a quadrupole, and for two d orbitals by a charge, a dipole, a quadrupole and a hexadecapole.²

The charge density overlap on a centre \mathbf{P} is then distributed to a new site \mathbf{S} (equation 3.3),

$$Q_{lm}(\mathbf{S}) = \sum_{k=0}^l \sum_{q=-k}^k \left[\binom{l+m}{k+q} \binom{l-m}{k-q} \right]^{\frac{1}{2}} Q_{kq}(\mathbf{P}) Q_{l-k, m-q}(\mathbf{S}-\mathbf{P}) \quad (3.3)$$

where Q denotes the multipole moments around a centre,

q and m represent the components of the multipole moment,

k and l describe the rank of the multipole moment.¹

Providing that sufficient expansion sites and orders of multipole are used, it should be possible to describe the molecular charge density distribution to the accuracy of the wavefunction. The electrostatic potential is calculated as follows (equation 3.4),

$$V(\mathbf{r}) = \sum_{lm} |\mathbf{r}-\mathbf{S}|^{-l-1} C_{lm}(\mathbf{r}-\mathbf{S}) Q_{lm}(\mathbf{S}) \quad (3.4)$$

where $|\mathbf{r}-\mathbf{S}|$ is the separation of the sites at which the potential is evaluated from the centre \mathbf{S} .

In order for this series to converge, the following condition must apply (equation 3.5),

$$|\mathbf{r}-\mathbf{s}| \gg |\mathbf{S}-\mathbf{P}| \quad (3.5)$$

This means that the points at which the potential is to be evaluated must be further away from \mathbf{S} than any of the centres \mathbf{P} , and thus the multipoles should not be shifted too far away from the original site \mathbf{P} . This condition is satisfied by choosing \mathbf{P} to be the atomic nuclei.²

Using this method, the distributed multipoles can give an exact representation of the electrostatic potential obtained from the *ab initio* charge density of the region that is being studied.⁶

A limitation to the technique is that it appears that the electrostatic energy obtained by a converged distributed point-multipolar distribution using *equation 3.4* is not equal to that obtained over the full spatial charge distribution using *equation 3.1*. The difference between these potentials is defined as the penetration energy. However, this quantity is a short-range effect that decays exponentially with separation and is empirically incorporated into the repulsion potential, with no significant effects on the orientation dependence of the electrostatic potential.²

3.2 Methodology

3.2.1 Procedure

The electrostatic potential around the formamide, (methyl)acetamide dimer and (methyl)acetamide trimer molecules were calculated using positive and negative point charge ‘probes’ (that is, H^+ and O^- ions). These probes were used to determine the potentials around these molecules by placing them at positions relative to the molecule that would be occupied by H and N and O and C atoms respectively in a longer (methyl)acetamide chain. The electrostatic potential was then calculated between the probe and the molecule. Three sets of electrostatic potentials were calculated:

- i. The electrostatic potential around the formamide, (methyl)acetamide dimer and (methyl)acetamide trimer molecules with the N-H bond at the equilibrium length in the dimer and trimer molecules keeping the N...O distance fixed (*figures 3.1, 3.2 and 3.3*),
- ii. The electrostatic potential around the monomer unit with the point charge probes placed in the same relative positions but a monomer unit away (*figure 3.4*),
- iii. The electrostatic potential around the dimer unit with the point charge probes in the same positions but with the H atom at different positions along the fixed N...O vector, keeping all other distances fixed.

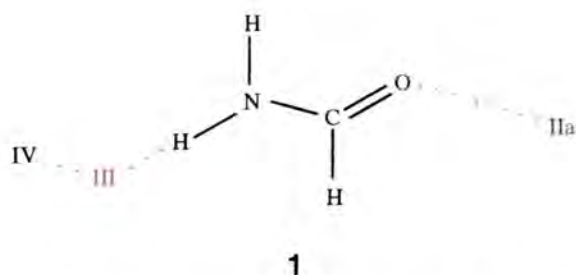


Figure 3.1 Formamide, with the positions of the probes shown. Position Ia represents the potential position of an H atom, IIa an N atom, III an O atom and IV a C atom.

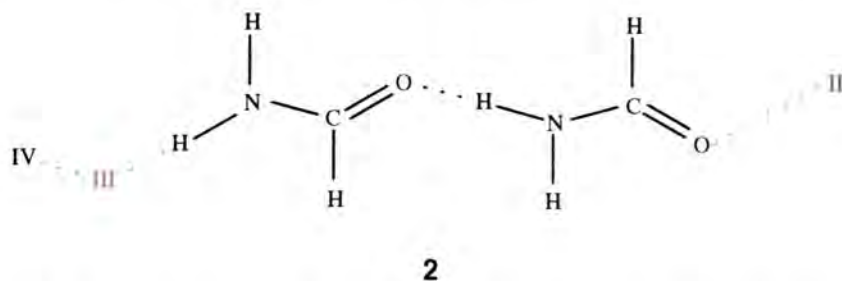


Figure 3.2 The (methyl)acetamide dimer, with the positions of the probes shown. Position I represents the potential position of an H atom, II an N atom, III an O atom and IV a C atom.

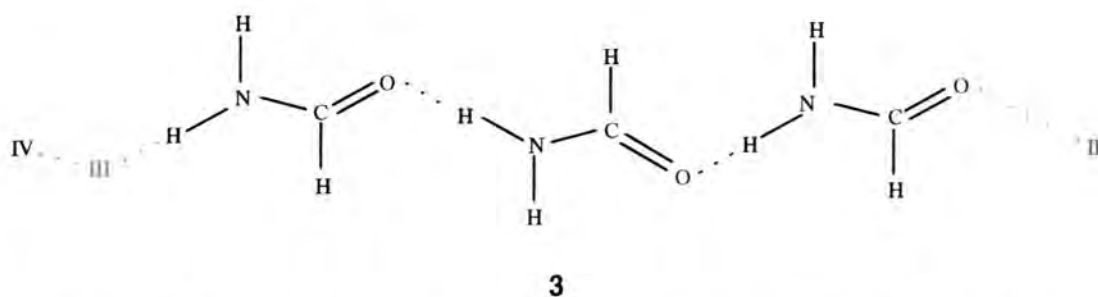


Figure 3.3 The (methyl)acetamide trimer, with the positions of the probes shown. Position I represents the potential position of an H atom, II an N atom, III an O atom and IV a C atom.

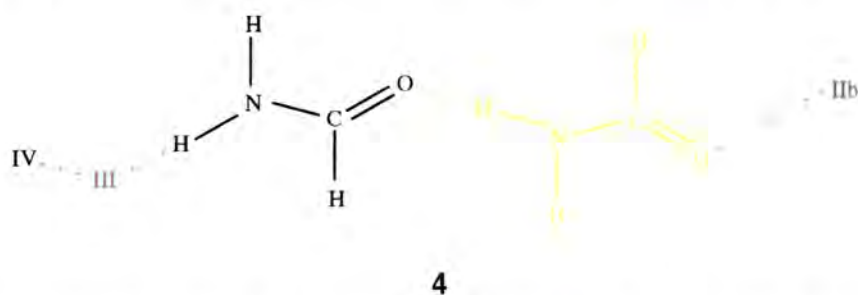


Figure 3.4 Formamide, with the positions of the probes shown. Position Ib represents the potential position of an H atom, IIb an N atom, III an O atom and IV a C atom. The 'ghost' monomer is indicated in yellow.

3.2.2 Computation

The program *CADPAC* (*Cambridge Analytical Derivatives package, UNIX version, issue 6*)⁷ was used to perform the DMA on the formamide, (methyl)acetamide dimer and (methyl)acetamide trimer molecules based on wavefunctions calculated at the MP2 level of theory using the 6-311G** basis set. Multipoles up to hexadecapole were calculated (all terms up to R^{-5}). Subsequent calculations of the electrostatic potential around these molecules were performed using the program *ORIENT* (*version 3.2*).⁸

3.3 Results and Discussion

3.3.1 Additivity of the monomer units

The effects of adding monomer units on the electrostatic potential are shown in *tables 3.1* and *3.2* and *figures 3.5, 3.6* and *3.7*. From *table 3.1* it can be seen that the electrostatic potential for **2** with the positive point charge probe at position **I** is -194.86177425 kJ mol⁻¹. To calculate the effect of the second monomer unit on the potential, the potentials for **1** and **4** with the positive point charge probes at Ia and Ib respectively are combined to give a value of $-(162.46023397 + 19.0860804)$ kJ mol⁻¹ = -181.54631438 kJ mol⁻¹. The difference between these two potentials is -13.31545987 kJ mol⁻¹. This residual energy after addition of a monomer unit is the stabilisation energy due to the rearrangement of charge within the dimer relative to formamide. The stabilisation energy is generally between 10 and 20 kJ mol⁻¹ for similar systems.²

Similarly, the electrostatic potential for **2** with the positive point charge probe at position **II** is -106.22887839 kJ mol⁻¹. The combination of the potentials for **1** and **4** with the positive point charge probes at IIa and IIb respectively is $-(78.46244928 + 14.97649864)$ kJ mol⁻¹ = -93.43894792 kJ mol⁻¹. The stabilisation energy due to the rearrangement of charge within the dimer is the difference between these two potentials, and is equal to -12.78993047 kJ mol⁻¹. The results from these analyses indicate that the monomer units are indeed additive, and this is further illustrated by the similarity of the potential distributions in *figures 3.5* and *3.6*. The potential for the (methyl)acetamide trimer molecule is also shown in *figure 3.7* for comparison.

The electrostatic potentials after minimisation are presented in *table 3.2* for comparison. As expected, the electrostatic potentials after minimisation are the same for all point charge positions in each of the three systems.

Table 3.1 Electrostatic potentials at fixed geometry (before minimisation) for the formamide, (methyl)acetamide dimer and (methyl)acetamide trimer molecules with point charges at N, H, C and O atom positions relative to the molecules

Probe position	Formamide	The (methyl)acetamide dimer	The (methyl)acetamide trimer
I	-	-194.86177425	-217.72085981
Ia	-162.46023397	-	-
Ib	-19.08608041	-	-
II	-	-106.22887839	-117.76796938
IIa	-78.46244928	-	-
IIb	-14.97649864	-	-
III	-53.61391846	-75.48078104	-85.23721312
IV	-105.54403487	-136.59228566	-149.04591317

All energies in kJ mol^{-1} .

Table 3.2 Electrostatic potentials after minimisation for the formamide, (methyl)acetamide dimer and (methyl)acetamide trimer molecules with point charges at N, H, C and O atom positions relative to the molecules

Probe position	Formamide	The (methyl)acetamide dimer	The (methyl)acetamide trimer
I	-	-191.22760708	-205.74804785
Ia	-151.81160799	-	-
Ib	-151.81160799	-	-
II	-	-191.22760708	-205.74804785
IIa	-151.81160799	-	-
IIb	-151.81160799	-	-
III	-98.59342302	-129.02126889	-141.41162370
IV	-98.59342302	-129.02126889	-141.41162370

All energies in kJ mol^{-1} .

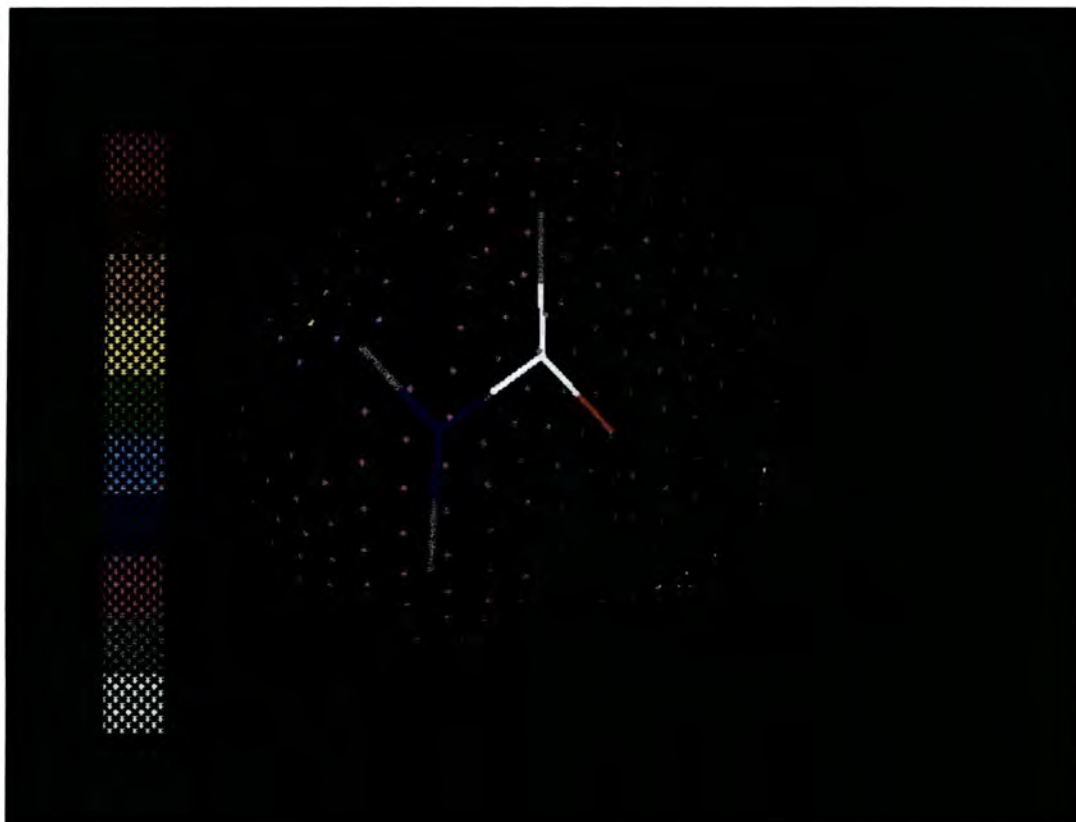


Figure 3.5 Electrostatic potential around the formamide molecule (key: white – low energy, red – high energy).

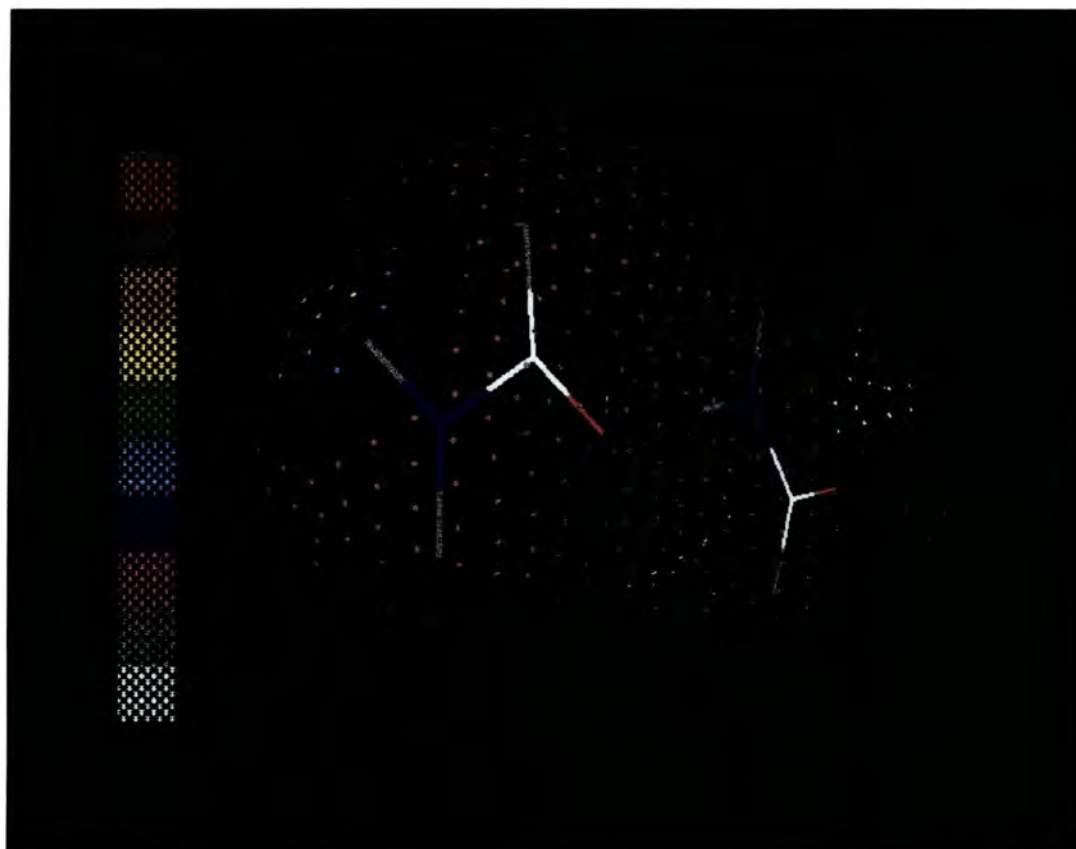


Figure 3.6 Electrostatic potential around the (methyl)acetamide dimer molecule (key: white – low energy, red – high energy).

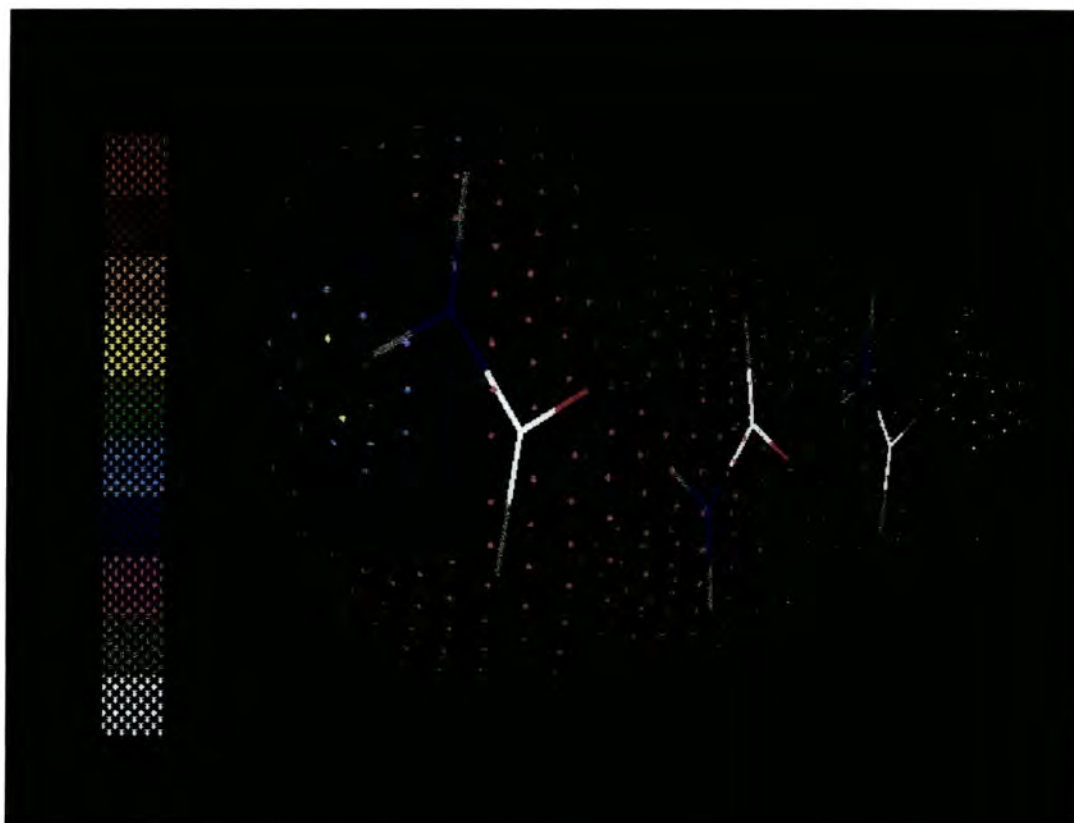


Figure 3.7 Electrostatic potential around the (methyl)acetamide trimer (key: white – low energy, red – high energy).

3.3.2 Is there cooperativity between two or more protons?

The results are presented in *tables 3.3* and *3.4* and *figures 3.8-3.17*. *Tables 3.3* and *3.4* show the difference in potentials at different points around the dimer molecule for a set of N-H distances before and after minimisation respectively. From both tables it can be seen that increasing the N-H distance results in increasingly negative electrostatic potentials, and this effect is represented pictorially in *figures 3.8-3.17*. This implies that there is a significant long-range effect as this distance is changed, which is due to a dipolar effect brought about by movement of the H atom away from the N atom. This motion results in an increasingly negative dipole on the N atom that is stabilised by the positive point charge.

Similarly, movement of the positive H atom along the N...O vector towards the O atom results in an increasingly positive dipole on the O atom that is stabilised by the negative point charge. As in *table 3.2*, minimisation results in potentials that are the same for all point charge positions, and this is shown in *table 3.4*. It can be concluded from these results that moving the H atom along the N...O vector facilitates a significant change in the electrostatic potential around the molecule. These results indicate that cooperative effects are present in the trimer molecule, and by extrapolation, the tetramer and pentamer (methyl)acetamide systems.

Table 3.3 Electrostatic potentials for the (methyl)acetamide dimer for different H atom positions along the N...O vector at fixed geometry (before minimisation)

N-H distance	Probe position			
	I	II	III	IV
0.37	-182.21256537	-92.96528449	-122.63795932	-66.03201722
0.58	-188.95730101	-97.10890508	-126.07509848	-68.39745435
0.79	-194.86177425	-100.89341987	-130.02523862	-71.07849721
1.00	-202.97083944	-106.22887839	-136.59228566	-75.48078104
1.21	-216.53764588	-115.12470035	-148.36288930	-83.31821043
1.43	-239.19253088	-129.80377810	-168.07479124	-96.40908969
1.64	-271.63349924	-150.63064629	-195.89044754	-114.88041243
1.85	-306.30850953	-172.84227751	-225.71324154	-134.68656921
2.06	-330.92426270	-188.71601803	-248.13833555	-149.53955321
2.27	-344.25143082	-197.46913556	-262.34604443	-158.87501343

All energies in kJ mol^{-1} , all distances in angstroms.

The entry in bold type is the electrostatic potential for the (methyl)acetamide dimer with the H atom at its equilibrium position.

Table 3.4 Electrostatic potentials for the (methyl)acetamide dimer for different H atom positions along the N...O vector after minimisation

N–H distance	Probe position			
	I	II	III	IV
0.37	-171.03556253	-171.03556253	-115.37681248	-115.37681248
0.58	-177.57487868	-177.57487868	-118.74064668	-118.74064668
0.79	-183.31994824	-183.31994824	-122.60382810	-122.60382810
1.00	-191.22760708	-191.22760708	-129.02126889	-129.02126889
1.21	-204.45177406	-204.45177406	-140.52200952	-140.52200952
1.43	-226.51872626	-226.51872626	-159.79522452	-159.79522452
1.64	-258.12540806	-258.12540807	-187.02982978	-187.02982978
1.85	-291.95476475	-291.95476475	-216.27143522	-216.27143522
2.06	-316.01869234	-316.01869235	-238.27431777	-238.27431777
2.27	-329.08141018	-329.08141018	-252.20780982	-252.20780982

All energies in kJ mol^{-1} , all distances in angstroms.

The entry in bold type is the electrostatic potential for the (methyl)acetamide dimer with the H atom at its equilibrium position.

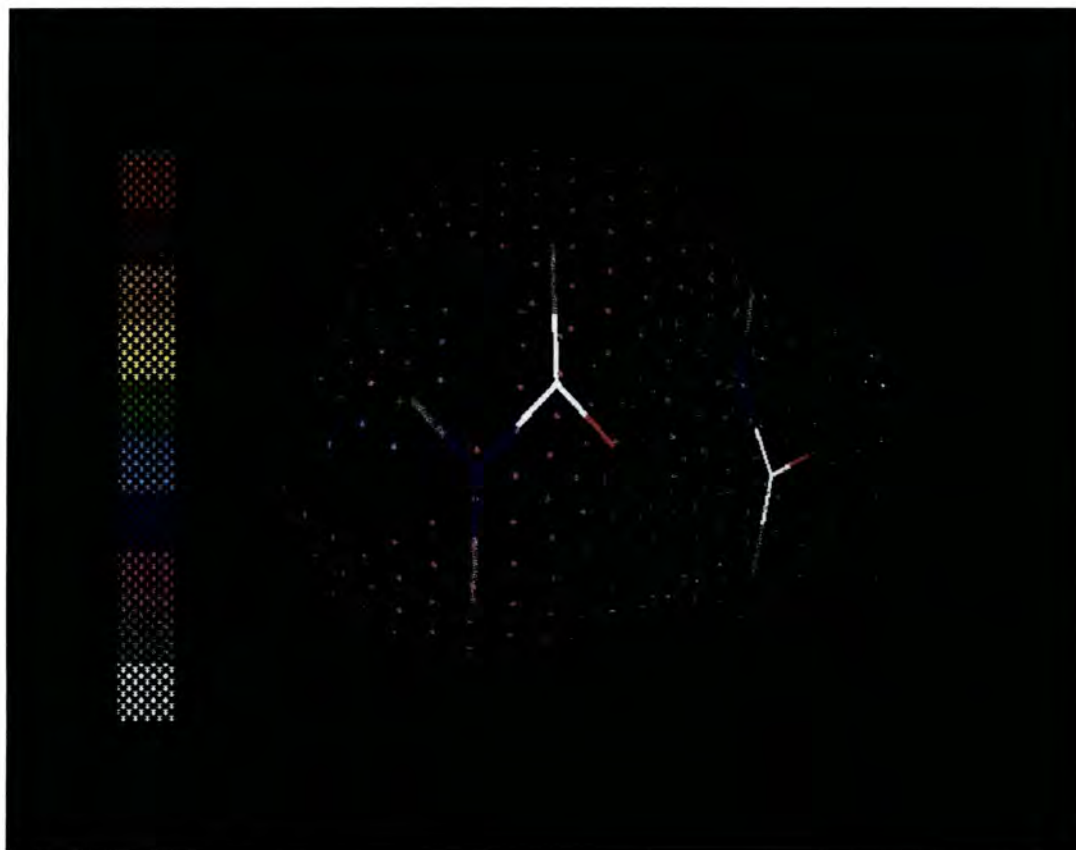


Figure 3.8 Electrostatic potential around the (methyl)acetamide dimer with the N–H separation at 0.37\AA (key: white – low energy, red – high energy).

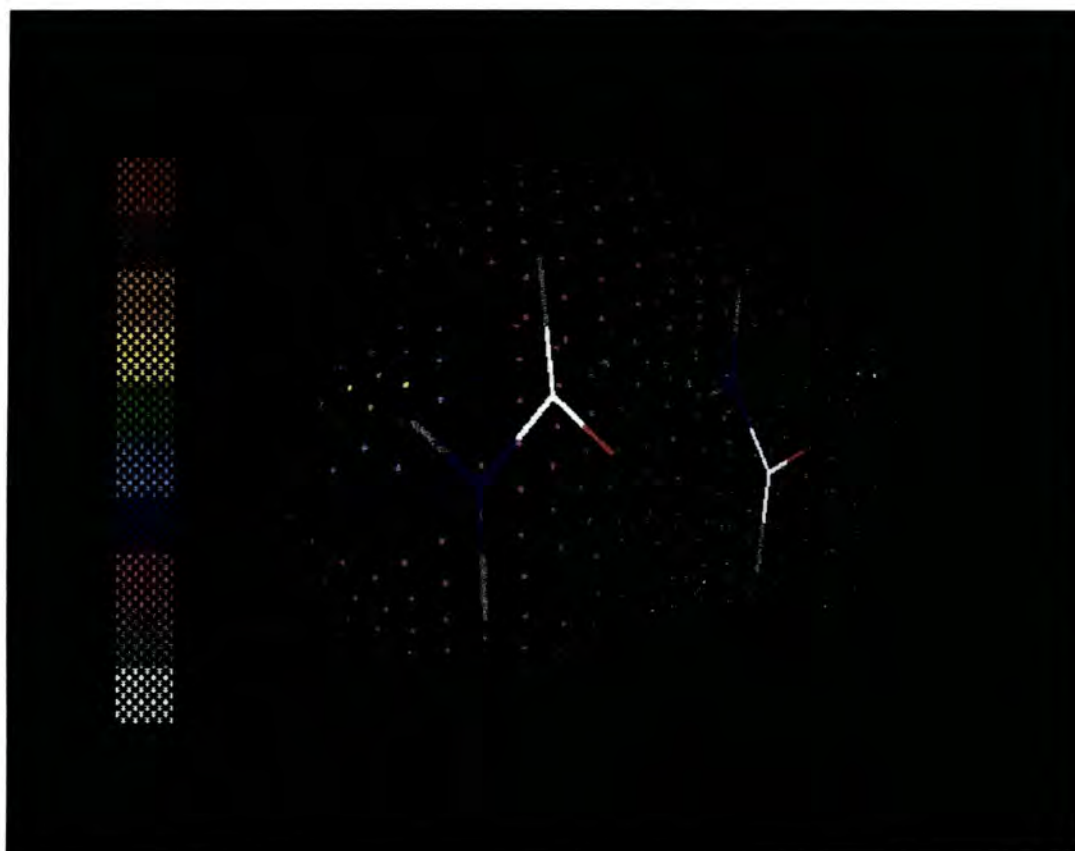


Figure 3.9 Electrostatic potential around the (methyl)acetamide dimer with the N-H separation at 0.58 Å (key: white – low energy, red – high energy).

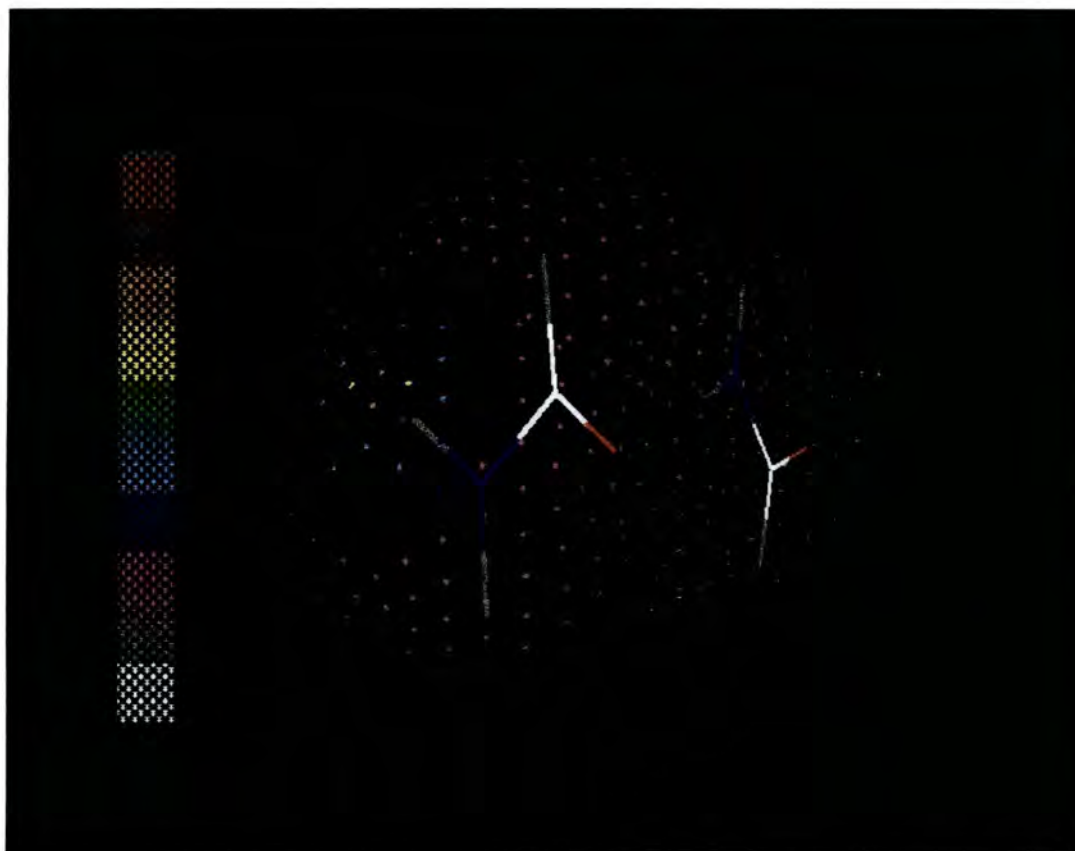


Figure 3.10 Electrostatic potential around the (methyl)acetamide dimer with the N-H separation at 0.79 Å (key: white – low energy, red – high energy).

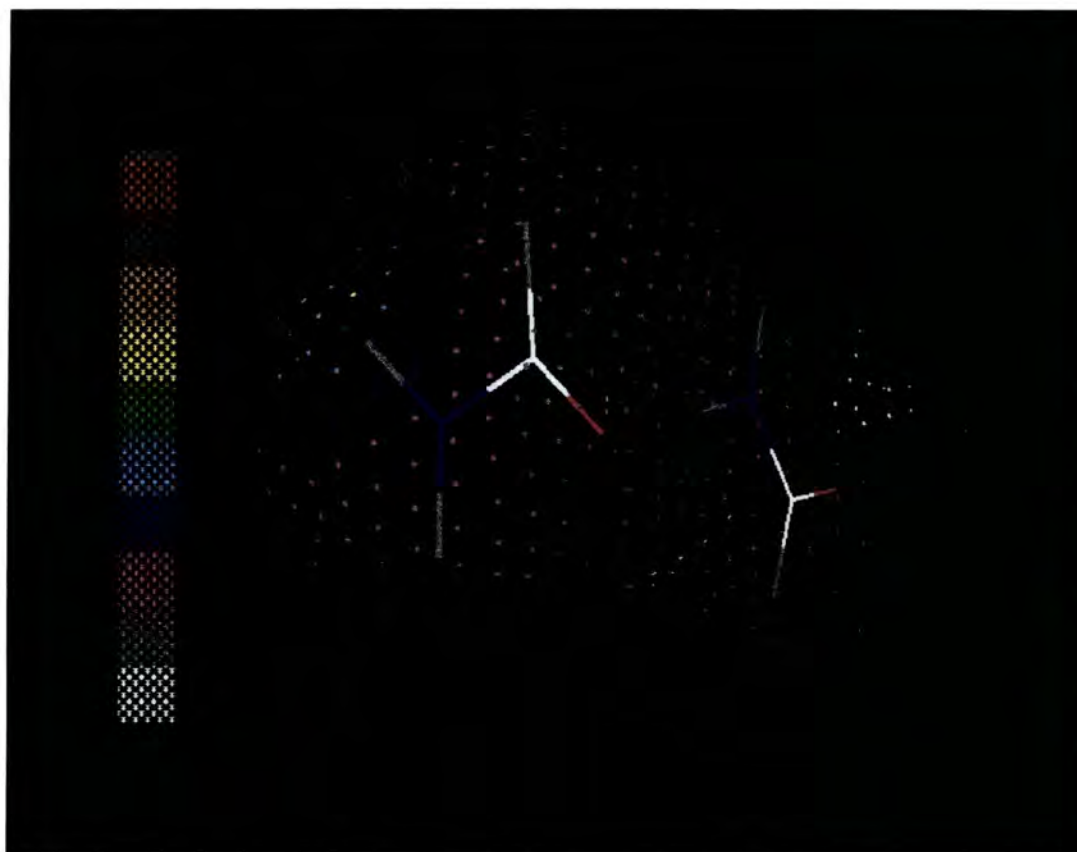


Figure 3.11 Electrostatic potential around the (methyl)acetamide dimer with the N-H separation at 1.00 Å (key: white – low energy, red – high energy).

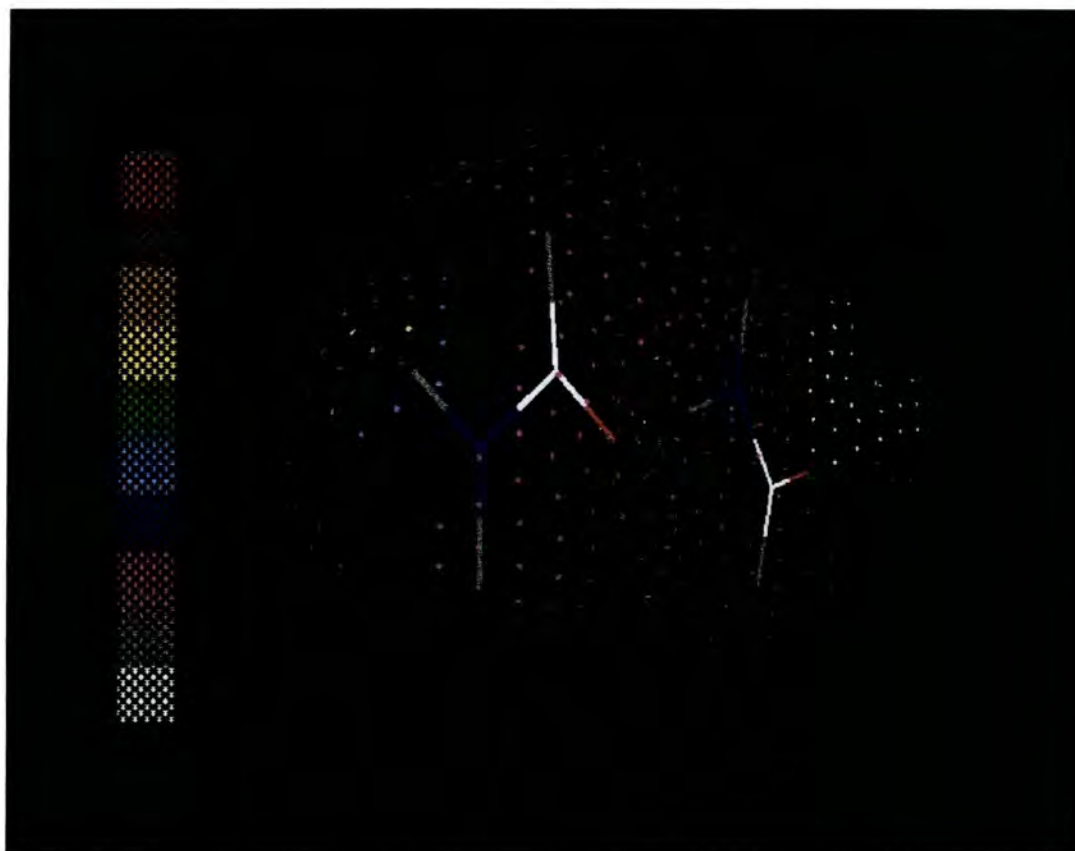


Figure 3.12 Electrostatic potential around the (methyl)acetamide dimer with the N–H separation at 1.21 Å (key: white – low energy, red – high energy).

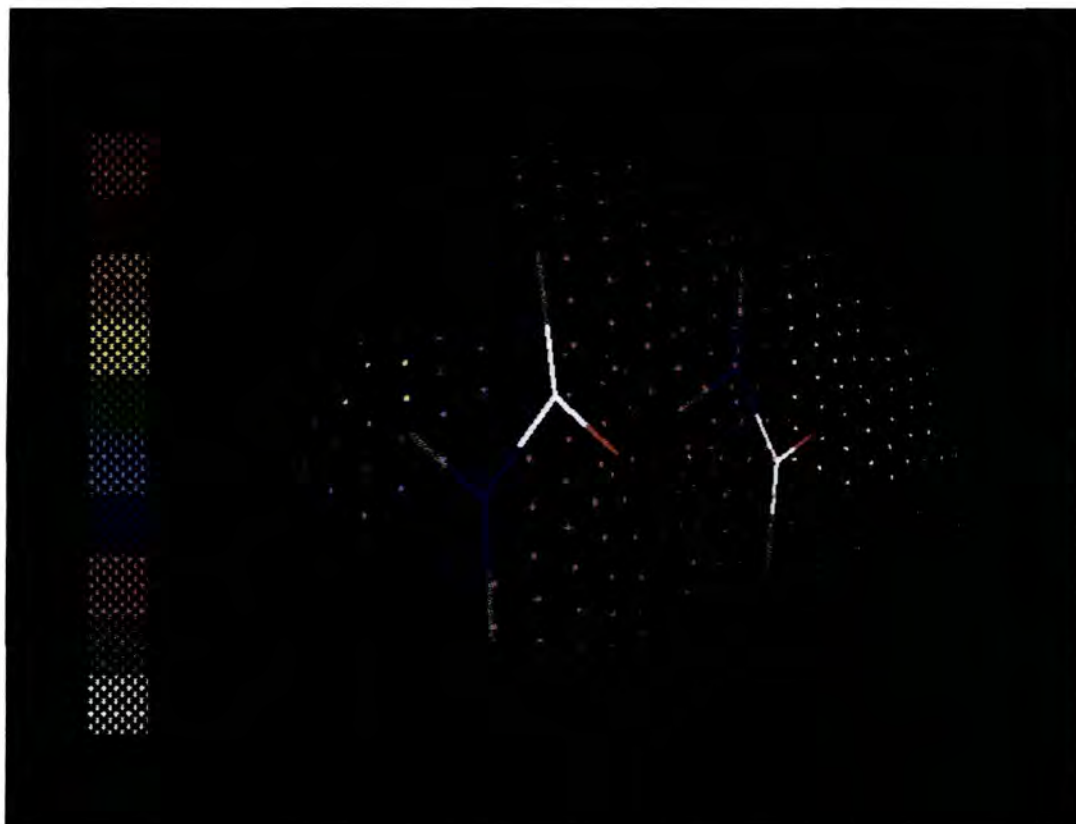


Figure 3.13 Electrostatic potential around the (methyl)acetamide dimer with the N–H separation at 1.43 Å (key: white – low energy, red – high energy).

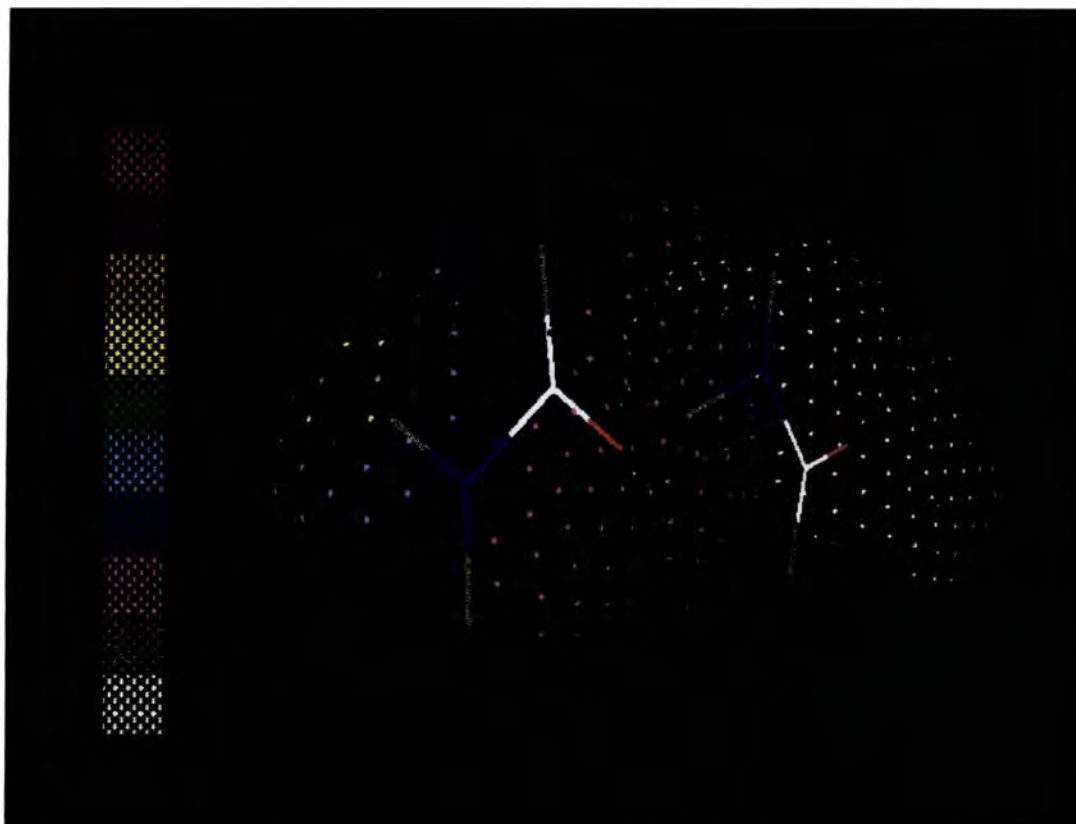


Figure 3.14 Electrostatic potential around the (methyl)acetamide dimer with the N-H separation at 1.64 Å (key: white – low energy, red – high energy).

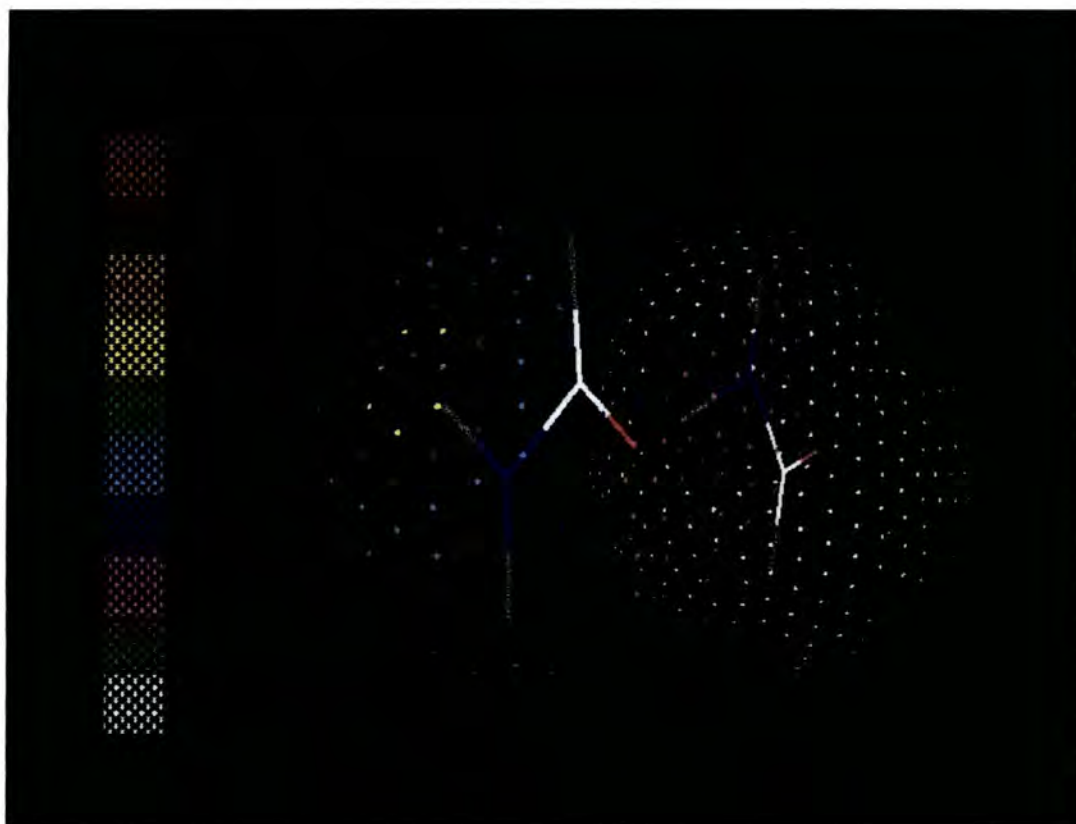


Figure 3.15 Electrostatic potential around the (methyl)acetamide dimer with the N-H separation at 1.85 Å (key: white – low energy, red – high energy).

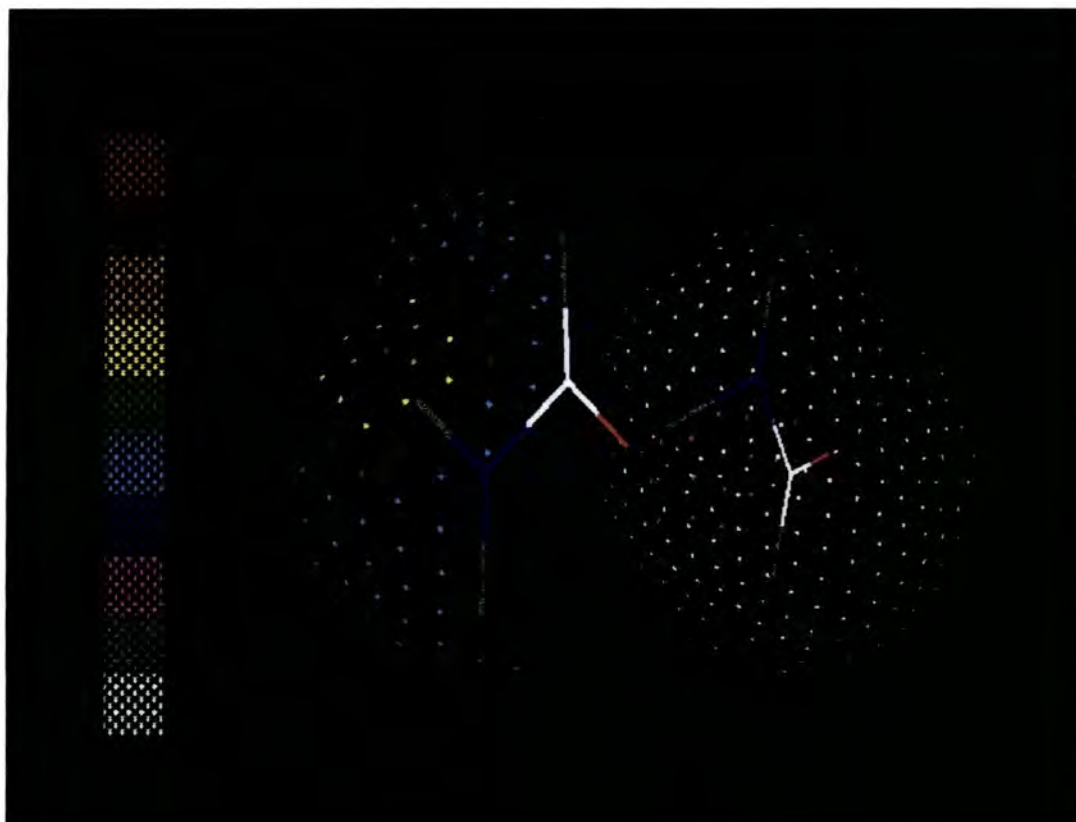


Figure 3.16 Electrostatic potential around the (methyl)acetamide dimer with the N-H separation at 2.06 Å (key: white – low energy, red – high energy).

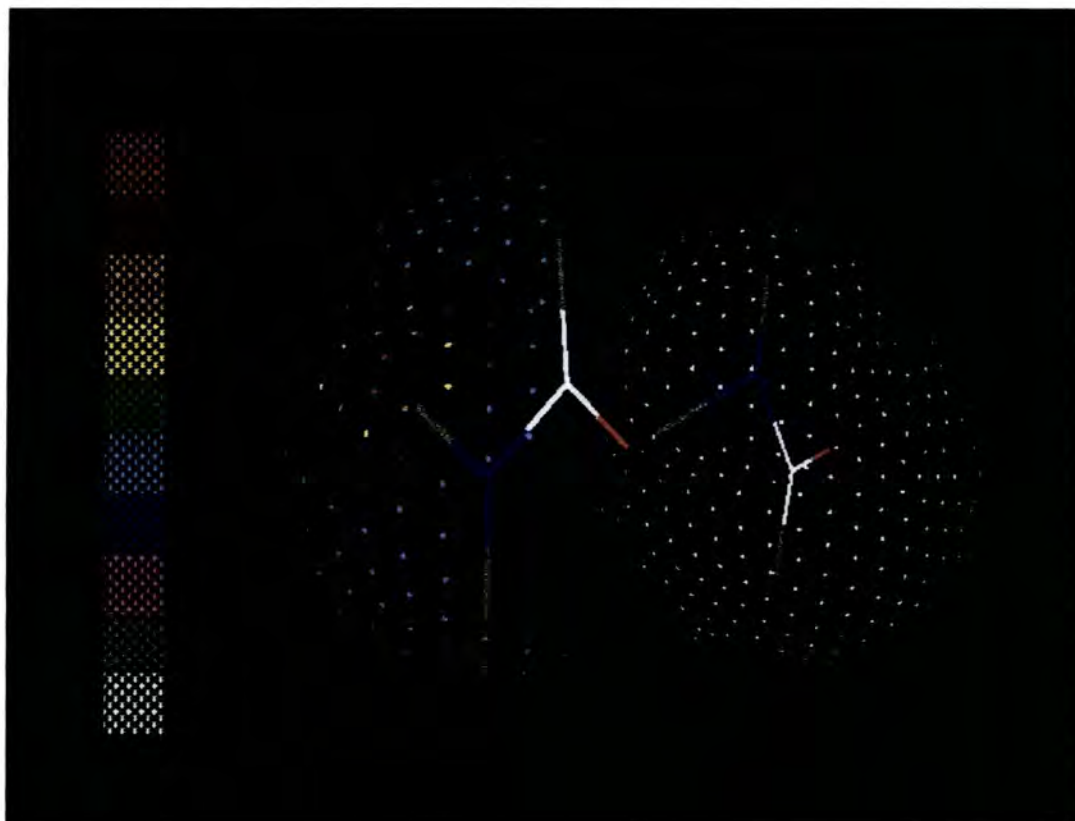


Figure 3.17 Electrostatic potential around the (methyl)acetamide dimer with the N-H separation at 2.27 Å (key: white – low energy, red – high energy).

3.3.3 Stability of the system to the movement of the proton

Tables 3.5 and 3.6 show the shift in the X and Y coordinates of the probe atoms in the Z plane after minimisation of **2**. There is no significant change in the position of the probes (to 1 decimal place) as the N–H distance is changed, and this indicates that the position of the minima of the electrostatic potentials also remains unchanged. The slight fluctuation in the probe coordinates is symptomatic of local changes in position within the potential wells with the actual minima positions remaining unchanged as the distance is varied. These results indicate that the system is stable to the effect of changing the N–H separation.

Table 3.5 X coordinates of the point charges after minimisation of **2**

N-H distance	Probe position			
	I	II	III	IV
0.37	-5.2436332	-5.6585908	6.1031022	6.7231809
0.58	-5.2428967	-5.6578624	6.1016300	6.7217326
0.79	-5.2434747	-5.6584387	6.1000094	6.7201348
1.00	-5.2439203	-5.6588833	6.0975846	6.7177276
1.21	-5.2436536	-5.6586205	6.0937506	6.7139017
1.43	-5.2416101	-5.6565940	6.0879816	6.7081277
1.64	-5.2369326	-5.6519446	6.0804756	6.7006051
1.85	-5.2307323	-5.6458016	6.0730844	6.6931975
2.06	-5.2253358	-5.6404510	6.0681366	6.6882491
2.27	-5.2214209	-5.6365678	6.0655436	6.6856710

All distances in angstroms.

Table 3.6 Y coordinates of the point charges after minimisation of **2**

N-H distance	Probe position			
	I	II	III	IV
0.37	-1.0153818	-1.3773137	1.0318755	0.7404074
0.58	-1.0152607	-1.3772574	1.0316876	0.7402459
0.79	-1.0153121	-1.3774361	1.0314789	0.7400733
1.00	-1.0153425	-1.3775902	1.0311613	0.7398414
1.21	-1.0152703	-1.3776108	1.0306515	0.7395054
1.43	-1.0149526	-1.3773044	1.0298760	0.7390248
1.64	-1.0142774	-1.3765519	1.0288600	0.7384117
1.85	-1.0133972	-1.3754499	1.0278537	0.7378017
2.06	-1.0126347	-1.3745233	1.0271755	0.7373709
2.27	-1.0120839	-1.3738898	1.0268165	0.7371158

All distances in angstroms.

3.4 References

- [1] A. J. Stone, "*The Theory of Intermolecular Forces*", chapter 1, (Clarendon Press, 1996)
- [2] S. L. Price, 'Electrostatic forces in molecular interactions' in "*Molecular Interactions: From van der Waals to strongly Bound Complexes*" ed. S. Scheiner, (Wiley, 1997)
- [3] Stone, A. J. *Chem. Phys. Lett.* **83**, 233, (1981)
- [4] Stone, A. J., Alderton, M. *Molec. Phys.* **56**, (5), 1047, (1985)
- [5] Price, S. L., Stone, A. J. *J. Chem. Soc. Faraday Trans.* **88**, (13), 1755, (1992)
- [6] Faerman, C. H., Price, S. L. *J. Am. Chem. Soc.* **112**, 4915, (1990)
- [7] *CADPAC (The Cambridge Analytical Data Package, Issue 6, University of Cambridge, Cambridge, UK)* R. D. Amos (1994)
- [8] *ORIENT* version 3.2, developed by A. J. Stone, with contributions from A. Dullweber, P. L. A. Popelier, D. J. Wales, (December 1995)

CHAPTER 4

Conclusions

The results obtained for proton transfer in the system are inconclusive. The data from the *ab initio* calculations indicates that proton transfer does occur in the model (methyl)acetamide dimer system studied, but only at monomer separations of 3.2 – 3.4 Å. It is unlikely that this is the separation at which the proton transfer occurs in nature, although a re-determination of the crystal structure would provide a better benchmark to the monomer separation in the crystal than the one currently available. There are a number of reasons why the calculations on the system could have produced these inconclusive results.

The first could be due to the fact that the basis sets or level of theory used for the calculations are inadequate. The results from the counterpoise-corrected data suggest that the size of the basis set used for the dimer calculations at the different monomer separations is inadequate, and this is illustrated by the comparison with the counterpoise-corrected data for the larger basis set. To decrease the effects of basis set superposition error it would be necessary to utilise a large customised basis set incorporating diffuse functions on the heavy atoms. However, the comparison of the counterpoise-corrected data of the two basis sets indicate that the level of theory used (MP2) is sufficient, although the data for the corrected curves at the latter repulsive end of the potential well indicate that much investigation needs to be made into the correcting for the dissociation effect by improving the description of the electronic effects at the longest N–H separations.

The second could be due to deficiencies in the model used. Further calculations would have to be carried out with the methyl groups included in the molecules to assess the effect this has on the resulting potential energy surface. Also, the fact that gas-phase monomer geometries were fixed at the crystal structure separation and angle in the dimer without taking account of the influence of the

crystal field on the system in a quantitative way is unsatisfactory, as the calculations on the trimer, tetramer and pentamer only provide a loose and qualitative guide to the effect of modelling the dimer in a pseudo-crystalline environment, although this approach has been validated by the data from the distributed multipole analyses.

Thirdly, the calculations were done on the fixed geometry dimer, trimer, tetramer and pentamer geometries. For a fully comprehensive study, separate calculations would need to be done in which the intramolecular coordinates of the monomer units were optimised fully for each hydrogen position to enable a comparison with the proton transfer modelled in a frozen system. Nevertheless, studies on very similar systems by Scheiner *et. al.* have indicated that full monomer geometry optimisation along the transfer path has no significant effect on the resulting potential energy surface.

The results from the distributed multipole analysis, however have resulted in positive conclusions about the model used. The first is that the large difference between the formamide and dimer electrostatic potentials obtained is mainly due to the addition of the extra molecule. The rearrangement of charge in dimer formation has some effect, which will tend to stabilise the next H bond, but it can be assumed that addition of monomer units to the system will have no significant effects on the potential.

Secondly, the electrostatic potential around the dimer molecule is significantly affected by the movement of the H atom along the N...O vector. Thus the movement of one proton along a bond will significantly affect the environment of other hydrogen bonds in the molecule, implying that there are cooperative effects between the motions of the protons. Synchronicity of the protons in the systems with

two or more hydrogen bonds can therefore be assumed, and thus these findings validate the 'building block' approach to the study of the proton transfer.

Despite the deficiencies described the results presented indicate that proton transfer in *N*-methylacetamide is indeed governed by a double minimum potential well, and that improved *ab initio* calculations on the dimer taking into account quantitatively crystal field effects would enable a more comprehensive evaluation of the proton transfer. Currently, this has not been achieved by any other theoretical or experimental procedure, and the results from the vibrational spectra of *N*-methylacetamide by Fillaux *et. al.* have not described the proton transfer in other than a qualitative way.

An improved crystal structure determination would help in the comparison of experimental and theoretical data, although there are some practical difficulties due to the melting point (25 – 26°C) and hygroscopic nature of the compound. Ideally, data from neutron diffraction of the deuterated and non-deuterated compounds would allow an experimental investigation of the proton transfer. To allow the comparison of the spectroscopic and theoretical data, further work could include fitting the calculated vibrational levels to the double minimum potential and computing the vibrational corrections to the energy. The combination of these techniques would allow a detailed study of proton transfer in this compound, as well as perhaps giving insights into the strengths and weaknesses of the theoretical approach taken to study such a process.

CHAPTER 5

Additional Work:

**A theoretical study of the hydrogen bond
acceptor properties of divalent sulfur and oxygen**

5.1 Introduction

5.1.1 Previous work

The acceptor properties of sulfur in C=S systems has been of considerable interest due to their abundance in biological systems as diverse as amino acids and thiamine and as antibiotic agents in penicillins and cephalosporins. Until recently, the focus of research has not centred on the mechanism of hydrogen bond formation involving C=S.

Recent work by Allen *et. al.*,¹ has taken the form of studies of the Cambridge Structural Database (CSD) (Allen *et. al.* 1991)² system to determine the geometrical characteristics of inter- and intramolecular N,OH...S=C bonds in comparison with those of N,OH...O=C bonds. In addition to these studies, *ab initio* MO calculations of the residual atomic charges and residual electrostatic potentials were performed and were shown to corroborate the database results.

The main findings of this work were the following:

- i. The mean C=S bond length is much longer than the mean C=O bond length and spans a much broader distance range (*figure 5.1*). This is because oxygen is much more electronegative than sulfur³ and because the σ and π components of the C=S bond are weaker than those of the C=O bond.
- ii. The univalent S atom is a weaker hydrogen bond acceptor than the univalent O atom, and is only an effective acceptor when R_1, R_2 can form an extended delocalised system with C=S (*figure 5.2*) due to resonance-induced electronegativity. This is illustrated in *figure 5.3*.

iii. There are preferred intermolecular bonding angles for both C=S...H and C=O...H systems, and these are shown in *figures 5.4* and *5.5*. For the univalent sulfur systems, the more diffuse nature of the lone pair density results in a broader spread for θ (*figure 5.5*).



Relative strengths of C=S...H and C=O...H hydrogen bonds

• **Comparison of mean S...H and O...H distances (Å)**

Donor-H	$\Sigma \text{vdW} - d(\text{S} \dots \text{H})$	$\Sigma \text{vdW} - d(\text{O} \dots \text{H})$	D(O-S)
O-H	2.90 - 2.41 = 0.49	2.62 - 1.89 = 0.73	0.24
N-H	2.90 - 2.51 = 0.39	2.62 - 2.01 = 0.61	0.22

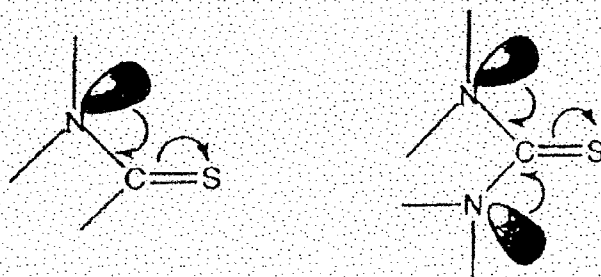
• **Competition for O-H and N-H donors**

Structures with	n(acceptors)	n(H-bonded)	
		C=S	C=O
(a) one C=S only	202	133(66%)	-----
(b) one C=O only	3549	-----	2342(66%)
(c) one C=S + one C=O only	81	34(42%)	58(72%)

Figure 5.1 The relative strengths of C=S...H and C=O...H hydrogen bonds

Resonance-induced H-bonding at S in $>C=S$

[Allen, Bird, Rowland & Raithby, *Acta Cryst*, B53, 660, 1997]



C=S,O distances (Å) and partial charges (q) on S and O in R1,R2 -- C=S,O systems

R1	R2	d(C=S)	q(S)	d(C=O)	q(O)
H	H	1.590	-0.023	1.210	-0.416
NH2	H	1.659	-0.270	1.224	-0.555
NH2	NH2	1.681	-0.390	1.221	-0.634

Figure 5.2 Resonance-induced hydrogen bonding at S in univalent sulfur systems

Percentage of S forming H-bonds as $d(C=S)$ increases

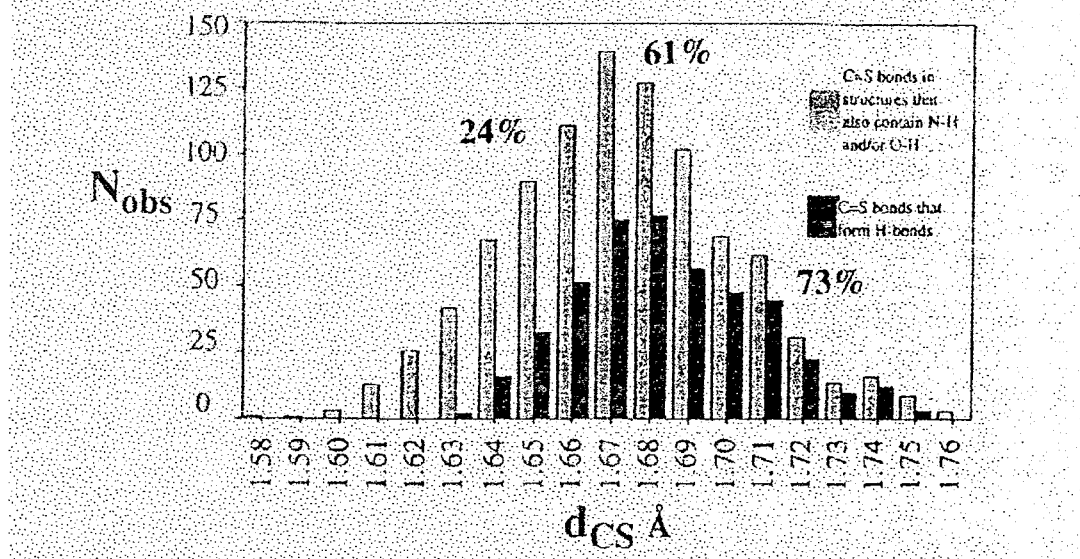


Figure 5.3 Percentage of S forming hydrogen bonds as $d(C=S)$ increases

Hydrogen bonding at univalent (=S) and (=O) acceptors

Directionality of H approach to S or O lone pair plane:

Circular histograms of rotation angle (ϕ), symmetrised data

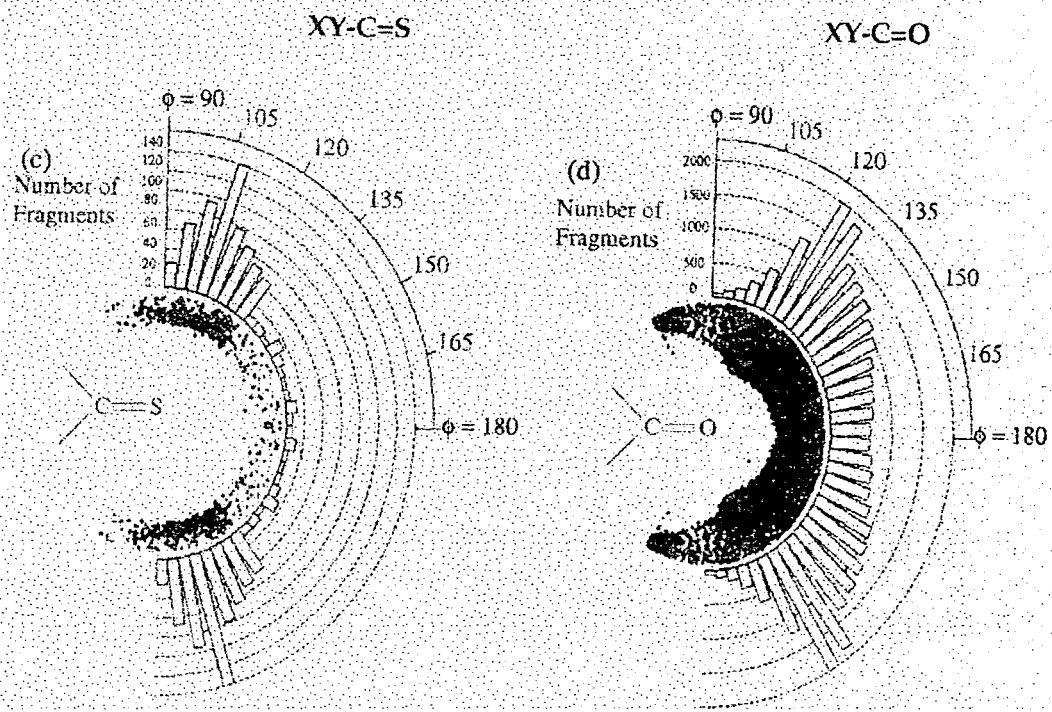


Figure 5.4 Histograms of rotation angle ϕ (in-plane angle between donor and acceptor molecules) for univalent S and O acceptors

Hydrogen bonding at univalent (=S) and (=O) acceptors

Directionality of H approach to S or O lone pair plane:

Circular histograms of angle of elevation (θ), symmetrised data

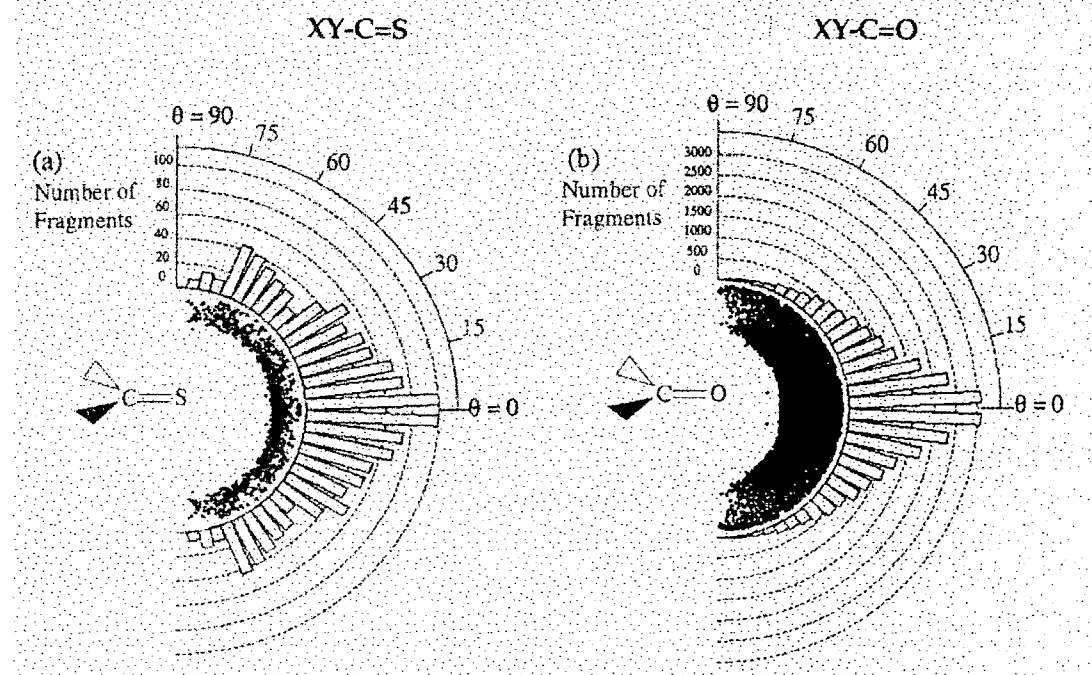


Figure 5.5 Histograms of elevation angle θ (out-of-plane angle between donor and acceptor molecules) for univalent S and O acceptors

5.1.2 IMPT calculations of the acceptor properties of C=S and C=O systems

To enable a comparison of the findings of Allen *et. al.*¹, the following features were investigated by *ab initio* calculations using the intermolecular perturbation theory (IMPT) to calculate the interaction between the donor and acceptor molecules. IMPT incorporates intermolecular forces and the effects of electron correlation in a single framework.⁴

The effects investigated were the following:

- i. The dependence of the interaction energy on the angle φ and on the substituents R_1, R_2 for the C=S...H and C=O...H systems.

- ii. The dependence of the strength of the interaction on the S...H and O...H for the thiourea / urea – methanol systems.

- iii. The dependence of the interaction energy on the angle θ for the thiourea / urea – methanol systems.

These should provide further insight into the findings of Allen *et. al.* by providing a theoretical comparison with the experimental database results.

5.2 Methodology

5.2.1 Procedure

Table 5.1 shows the substituents of the compounds investigated. The interaction energies of all of these compounds were determined as a function of φ , for angles of 80° to 135° for the thiourea systems and angles of 95° to 140° for the urea systems. The energies were measured in five degree increments and also in one degree increments around the optimum value for φ .

The dependence of the energies on the S...H separation was investigated in 0.05 \AA increments for the thiourea – methanol system for separations of $2.00 - 2.70 \text{ \AA}$. The interaction energy dependence on the O...H separation was also determined in 0.05 \AA increments for the urea – methanol system for separations of $1.55 - 2.25 \text{ \AA}$. In both cases, increments of 0.01 \AA were used around the optimum separations.

The dependence of the strength of the interaction on θ was studied over a range of $0 - 90^\circ$ for the thiourea – methanol and urea – methanol systems.

IMPT calculations of $>C=S...H-O$ and $>C=O...H-O$ interaction energies

Thiourea-S (urea-O) methanol model

Model geometries:

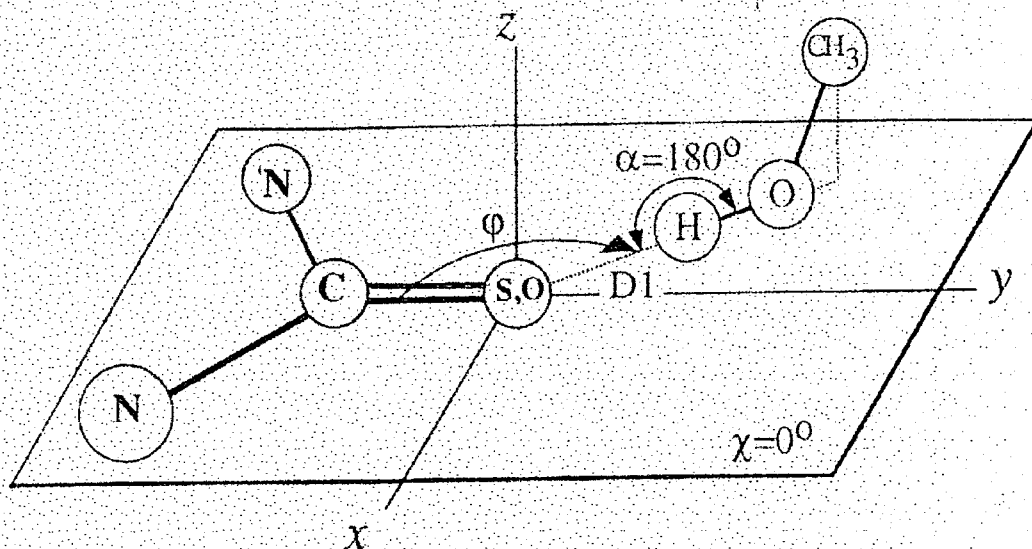


Figure 5.6 Representation of the thiourea / urea – methanol model

5.2.2 Computation

All calculations of the interaction energies were performed using the program *CADPAC*.⁵ The geometries of the thiourea, urea, methyl substituted thiourea, methyl substituted urea and methanol molecules were all optimised using the 6-31G* basis set at the MP2 level, and all subsequent calculations of the interaction energies were performed on these optimised geometries. No constraints were applied in any of the geometry optimisations.

5.3 Results and Discussion

The results are presented in *figures 5.7-5.13*. *Table 5.2* is a comparison of the results obtained from this study and from the database analyses of Allen *et. al.* It can be seen from *figures 5.9* and *5.10* that the optimum value of φ for the $(R_1, R_2)C=S\dots H$ system is 92° , and that for the $(R_1, R_2)C=O\dots H$ system is 110° . In both cases, the stronger interaction energies are obtained with the more electron-rich substituents which is expected because of the resonance-induced increase in electronegativity on the acceptor atoms. In all cases, the strength of the interaction for the $(R_1, R_2)C=O\dots H$ systems is greater than that for the corresponding $(R_1, R_2)C=S\dots H$ systems, expected because of the differences in electronegativity and electronic structure of the systems.

Figures 5.10 and *5.11* illustrate the change in the interaction energy with $S\dots H$ and $O\dots H$ separation respectively for the thiourea – methanol and urea – methanol interactions only. The optimum $S\dots H$ separation is 2.55 \AA , with the separations 2.4 and greater showing very similar interaction energies (within 1 kJ mol^{-1}). The optimum $O\dots H$ separation is 1.82 \AA , and in this case there is a very definite minimum in the energy curve corresponding to a narrow range of separations. This is expected from the database studies by Allen *et. al.*, illustrated by *figures 5.1* and *5.3*.

Figure 5.13 depicts the strength of the interaction energy as a function of the angle θ . For both the thiourea – methanol and urea – methanol systems the optimum value is 10° . Again, the spread of energies in the thiourea case is broader than that for the urea – methanol system, and this is due to the more diffuse nature of the lone pair density for $=S$. A discrepancy with the results of the database study is that values of θ were found to extend to $\pm 60-65^\circ$ for $=S\dots H$ systems. The results from the IMPT

calculations show that beyond 50°, the interaction energies are positive in the case of the methanol donor. Calculations involving a range of donor molecules would provide further information in this case.

The comparison of the results from this work and that of Allen *et. al.* in *table 5.2* appears to show significant discrepancies between the two sets of results. However, the difference in energies between the optimum calculated results and those from the database study in all the cases is not more than 1 kJ mol⁻¹, and can therefore be assumed not significant. The fact that the database study was done for a wide variety of donor and acceptor molecules and the calculations only for a few specified systems should account for this difference.

Table 5.2 Comparison of the optimum parameter values from the IMPT calculations and the database studies of Allen *et. al.* on thiourea / urea...H–O,N bonded systems

Parameter	Thiourea		Urea	
	IMPT results	Database studies	IMPT results	Database studies
φ	92	105-110	110	120-130
θ	10	0-5	10	0-5
$d(X...H)$	2.55	2.41	1.82	1.88

All bond lengths in angstroms, all bond angles in degrees.

IMPT calculations of urea-O...H-O interaction energy

[Allen, Amer & Howard, 1997, unpublished]

Interaction energy as a function of ϕ

Fixed parameters: $d(O...H) = 1.90 \text{ \AA}$, $\theta = 0^\circ$

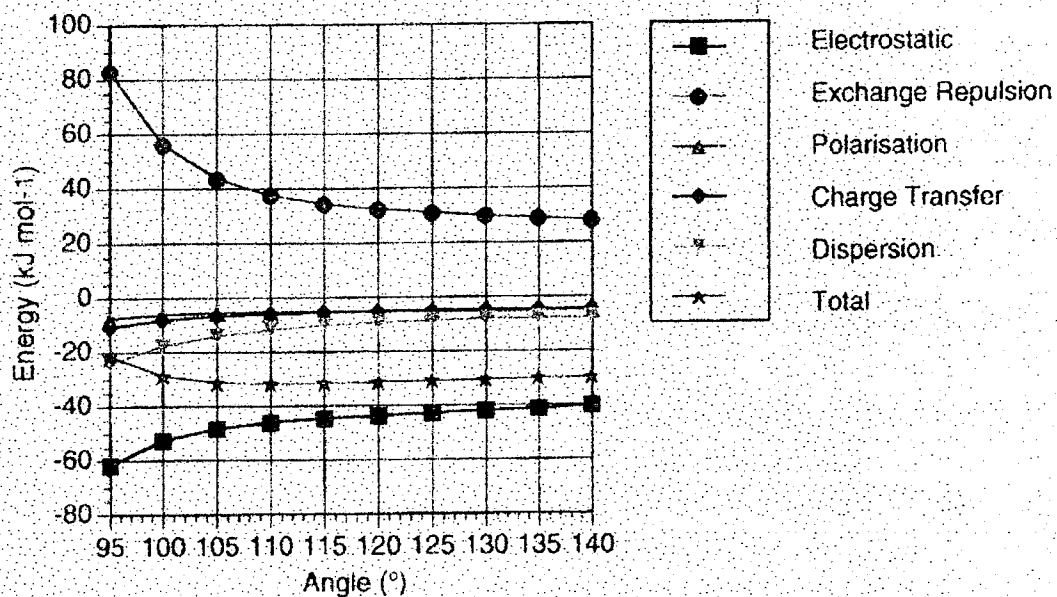


Figure 5.7 IMPT calculations of the thiourea – methanol interaction energy

IMPT calculations of thiourea-S...H-O interaction energy

[Allen, Amer & Howard, 1997, unpublished]

Interaction energy as a function of ϕ

Fixed parameters: $d(S...H) = 2.40\text{\AA}$, $\theta = 0^\circ$

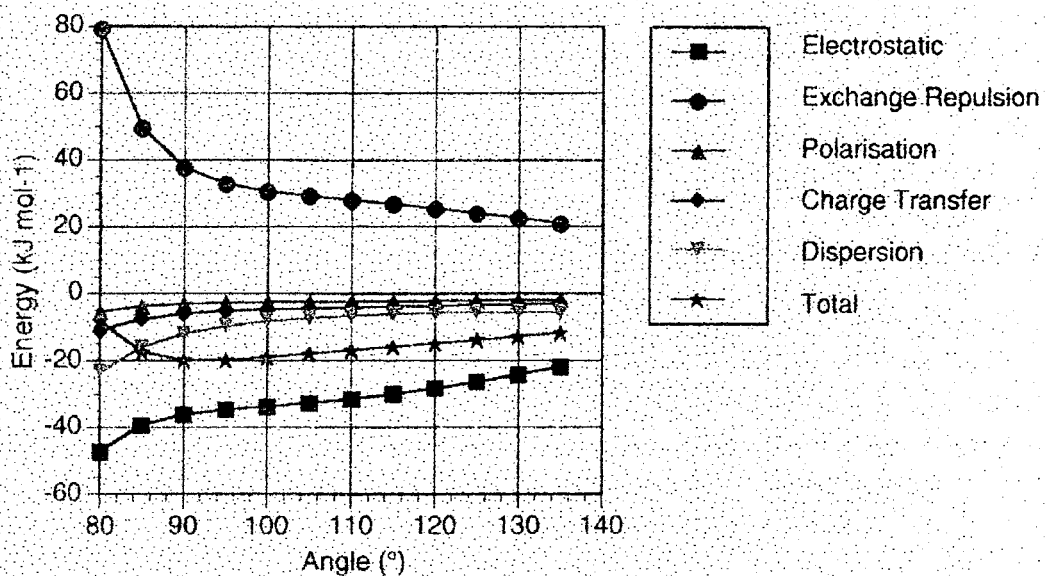


Figure 5.8 IMPT calculations of the urea – methanol interaction energy

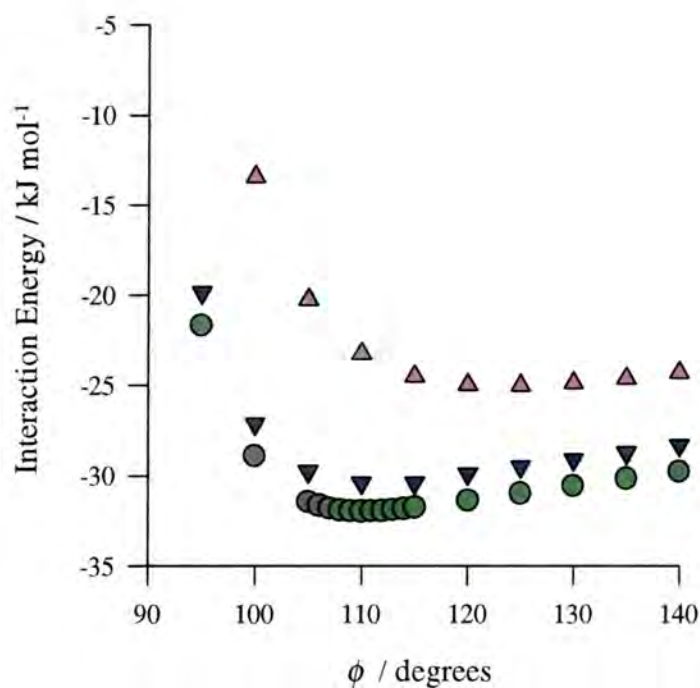


Figure 5.9 C=S...H interaction energies as a function of ϕ for thiourea (green), methyl substituted thiourea (blue) and dimethyl thioketone (pink)

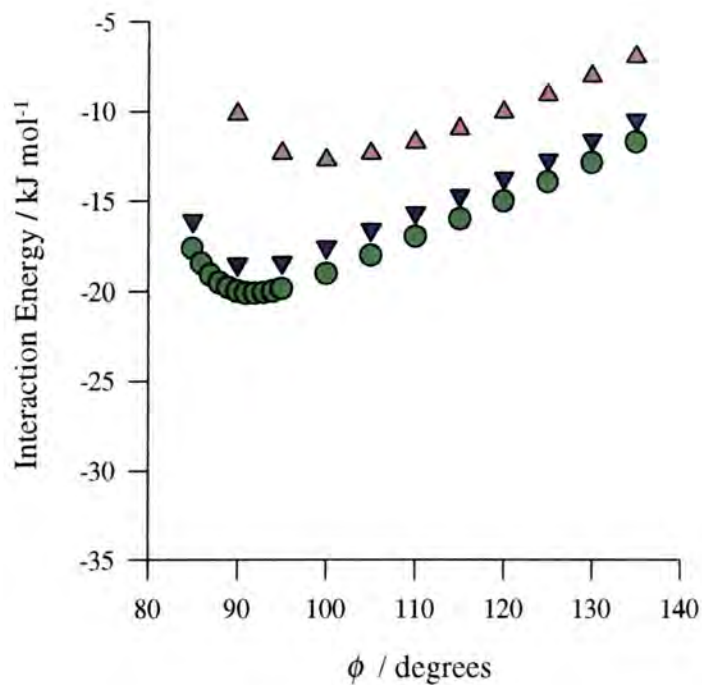


Figure 5.10 C=S...H interaction energies as a function of ϕ for urea (green), methyl substituted urea (blue) and dimethyl ketone (pink)

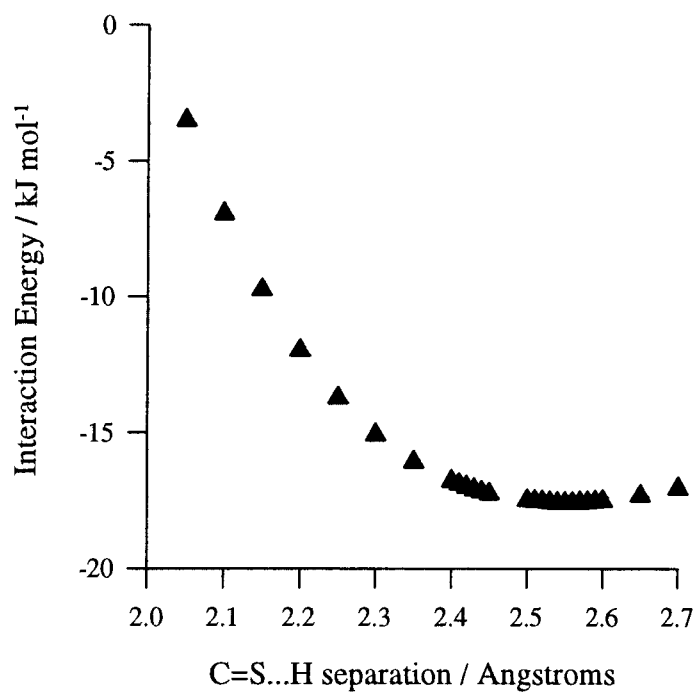


Figure 5.11 Change in thiourea – methanol interaction energy with C=S...H distance

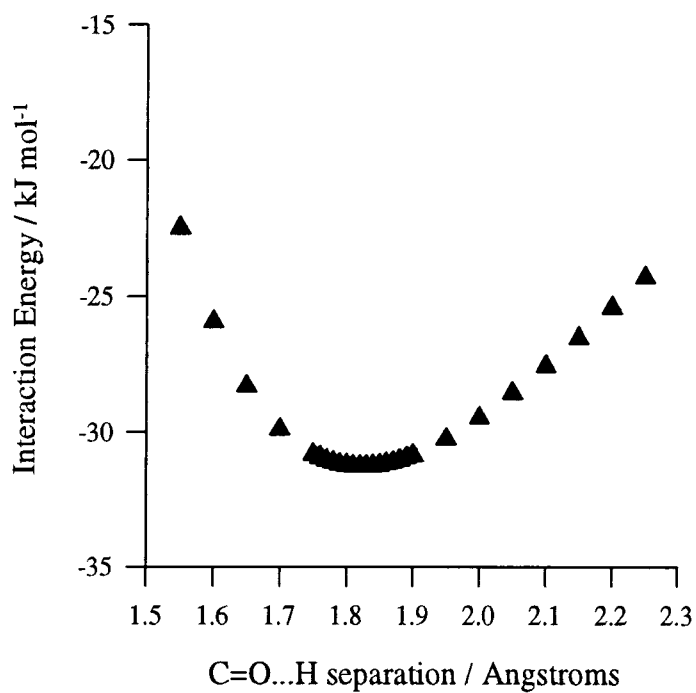


Figure 5.12 Change in urea – methanol interaction energy with C=O...H distance

5.4 Conclusions

The results of the IMPT calculations have been shown to corroborate the work of Allen *et. al.* and provide a theoretical basis for understanding the statistical distributions from experiment of the bond angles and separations for hydrogen bonded univalent sulfur and oxygen systems. Further theoretical calculations on a variety of similar systems would give additional insights into the bonding behaviour shown by the database results.

This work was presented by Dr. F. H. Allen at the 2nd Indaba Conference August 1997 and is currently being prepared for publication. *Figures 5.1-5.8* were used in the presentation and have been supplied by Dr. Allen.

5.5 References

- [1] Allen, F. H., Bird, C. M., Rowland, R. S., Raithby, P. *Acta Cryst.* **B 53**, 680, (1997)
- [2] Allen, F. H., Davies, J. E., Galloy, J. J., Johnson, O., Kennard, O., Macrae, C. F., Mitchell, E. M., Mitchell, G. F., Smith, J. M. and Watson, D. G. *J. Chem. Inf. Comput. Sci.* **31**, 187, (1991)
- [3] Pauling, L. *The Nature of the Chemical Bond*, (Ithaca: Cornell University Press, 1960)
- [4] Chalasinski, G., Szczesniak M. M. *Chem. Rev.* **94**, 1723, (1994)
- [5] *CADPAC (The Cambridge Analytical Data Package, Issue 6, University of Cambridge, Cambridge, UK)* Amos, R. D., (1994)

APPENDIX

Conferences and Courses

I Conferences

14-16 November 1996 – First European Charge Density Meeting, Les Prémontrés, Nancy, France.

7 February 1997 – Highlights of UK Chemistry Research and R&D by Young Chemists, The Royal Society, London.

14-17 April 1997 – British Crystallographic Association Annual Spring Meeting, Leeds. Poster Prize for “Best Neutron Related Poster, 1997”.

30 June – 2 July 1997 – The Royal Society of Chemistry Faraday Discussion No. 106, “Solid State Chemistry: New Opportunities from Computer Simulations”, University College, London.

II Courses

Graduate courses completed successfully at the University of Durham:

- i. 28 October – December 2 1996** – Practical nuclear magnetic resonance.
- ii. 29 October – December 3 1996** – Diffraction and scattering methods.
- iii. 6 February – March 19 1997** – Molecular modelling.

6-14 April 1997 – Sixth BCA Intensive Teaching School in X-ray Structure Analysis, University of Durham.

III Time Spent Away from Durham

20 - 24 January 1997 – Time spent at the Cambridge Crystallographic Database Centre, Cambridge learning how to use the program *CADPAC*.

5 – 26 July 1997 – Collaboration with Dr. Sally Price at University College, London using the Distributed Multipole Analysis (DMA) approach to provide further insights into proton transfer in *N*-methylacetamide.

